Climate Dynamics
https://doi.org/10.1007/s00382-019-04664-w

Regionalization and parameterization of a hydrologic model significantly affect the cascade of uncertainty in climate-impact projections

Saeid Ashraf Vaghefi[1] · Majid Iravani[2] · David Sauchyn[3] · Yuliya Andreichuk[3] · Greg Goss[4] · Monireh Faramarzi[1]

Received: 23 December 2017 / Accepted: 2 February 2019

Abstract
Climate-impact projections are subject to uncertainty arising from climate models, greenhouse gases emission scenarios, bias correction and downscaling methods (BCDS), and the impact models. We studied the effects of hydrological model parameterization and regionalization (HM-P and HM-R) on the cascade of uncertainty. We developed a new, widely-applicable approach that improves our understanding of how HM-P and HM-R along with other uncertainty drivers contribute to the overall uncertainty in climate-impact projections. We analyzed uncertainties arising from general circulation models (GCMs), representative concertation pathways, BCDS, evapotranspiration calculation methods, and specifically HM-P and HM-R. We used the Soil and Water Assessment Tool, a semi-physical process-based hydrologic model with a high capability of parameterization, to project blue and green water resources for historical (1983–2007), near future (2010–2035) and far future (2040–2065) periods in Alberta, a western province of Canada. We developed an Analysis of Variance (ANOVA)-Sequential Uncertainty Fitting Program approach, to decompose the overall uncertainty into contributions of single drivers using the projected blue and green water resources. The monthly analyses of projected water resources showed that HM-P and HM-R contribute 21–51% and 15–55% to the blue water, and 20–48% and 15–50% to the green water overall uncertainty in near future and far future, respectively. Overall, we found that in spring and summer seasons uncertainty arising from HM-P and HM-R dominates other uncertainty sources, e.g. GCMs. We also found that global climate models are another dominant source of uncertainty in future impact projections.

Keywords Uncertainty analysis · Uncertainty decomposition · Climate change · Natural climate variability · SWAT · ANOVA-SUFI-2

1 Introduction

Climate change as a major international environmental challenge is altering water resources. Numerous studies have assessed and quantified projections of future climate change and corresponding impacts on water balance components around the globe using various climate-impacts models (e.g. Abbaspour et al. 2009; Arnell 1999; Arnell and Gosling 2016; Asong et al. 2016; Barnett et al. 2005; Bavay et al. 2013; Beniston 2012; Erler and Peltier 2016; Gualdi et al. 2013; Maheu et al. 2016; Schar et al. 2016; Seneviratne et al. 2016; Vaghefi et al. 2017). Uncertainty is an inescapable characteristic of climate projections (Moss et al. 2010). It results from a lack of knowledge, lack of accurate input data, uncertain undrestanding of natural processes, and disagreement among experts (IPCC 2013; Morgan and Henrion 1990). Characterization and quantification of uncertainty

Electronic supplementary material The online version of this article (https://doi.org/10.1007/s00382-019-04664-w) contains supplementary material, which is available to authorized users.

✉ Saeid Ashraf Vaghefi
ashrafva@ualberta.ca

[1] Watershed Science and Modelling Laboratory, Department of Earth and Atmospheric Sciences, University of Alberta, Edmonton, AB T6G 2E3, Canada

[2] Alberta Biodiversity Monitoring Institute, University of Alberta, Edmonton, AB, Canada

[3] Prairie Adaptation Research Collaborative, University of Regina, Regina, SK, Canada

[4] Department of Biological Sciences, University of Alberta, Edmonton, AB, Canada

Published online: 09 February 2019

in climate change projections are essential for detection of changes in hydro-climatic variables and for effective climate change adaptation and mitigation strategies (IPCC 2013). Scientists and decision-makers agree that recommendations and adaptation scenarios based on a single climate model are unreliable. Consideration of multiple models under various possible futures climate should provide more reliable results albeit with higher uncertainty (Gobiet et al. 2014; Hallegatte 2009; O'Neill et al. 2014, 2017; van den Bergh 2017).

Projections of impacts of climate change on hydrologic regimes are prone to cascades of uncertainty due to natural variability of the climate, unknown future greenhouse gases emission trajectories, errors resulting from simplifications in global climate models (GCMs), dynamical or statistical downscaling methods, and hydrological models (Bosshard et al. 2013; Chen et al. 2011b; Gobiet et al. 2014). The numerous abbreviations used in this study are summarized in the Supplemental Information, Table SI.1.

A growing number of studies have considered multiple sources of uncertainty in modeling hydro-climatic impacts of climate change (Abbaspour et al. 2009; Bosshard et al. 2013; Chen et al. 2011b; Harding et al. 2012; Hewitt et al. 2016; Kay et al. 2009; Prudhomme and Davies 2009; Teklesadik et al. 2017; Vetter et al. 2015, 2017; Wilby and Harris 2006; Yip et al. 2011). Table 1 summarizes the different sources of uncertainty and the significant findings of each study. Most of the above-mentioned literature has documented the contribution of GCMs, greenhouse gases emission scenarios (GGES), downscaling (DS) and hydrological model structure (HM-S) components in the chain of uncertainties. However, there are only limited studies (e.g. Abbaspour et al. 2009; Poulin et al. 2011) which have quantified the uncertainty associated with hydrological model parameterization (HM-P) and regionalization (HM-R) on projected hydrological changes. In general, Table 1 shows that uncertainty due to the choice of GCMs is the dominant source in the chain of uncertainties. However, there is no agreement on the next major uncertainty sources. For instance, uncertainty due to the choice of DS, GGES, and selection of hydrological models (HM-S) have been reported as the second major uncertainty source in at least one of the reviewed studies in Table 1. Examination of Table 1 shows that the order of uncertainty sources (major to minor) varies spatially and temporally amongst the cases. More recently, studies have investigated multiple river basins covering various climatic conditions to quantify the contribution of different sources of uncertainty in the projection of hydrological changes (Hattermann et al. 2018; Vetter et al. 2015, 2017).

The studies in Table 1 have implemented different approaches for uncertainty analysis. Some have modeled uncertainty and demonstrated it as an uncertainty band (category 1), while others have quantified the contribution of individual uncertainty sources using different uncertainty decomposition methods (category 2). Some studies from the former category employed Sequential Uncertainty Fitting (SUFI-2) to capture the uncertainty of regionalization and parameterization of the hydrological models on water resources in different regions (Abbaspour et al. 2007; Faramarzi et al. 2009). These studies used the Soil and Water Assessment Tool (SWAT, Arnold et al. 1998, 2012) for projection of hydrological variables. Other studies in this category, i.e. Poulin et al. (2011), used a shuffled complex evolutionary algorithm (Duan et al. 1993) to analyze the parameter uncertainty of two hydrological models, namely HYDROTEL (Fortin et al. 2001) and HSAMI (Fortin 2000) in a snow-dominated river basin in Canada. For the latter category, Wilby and Harris (2006) used a probabilistic framework for assessing uncertainties in climate change impacts by applying a Monte Carlo approach to explore components of uncertainty in projected low river flow in the River Thames basin in Britain. Chen et al. (2011b), examined the effects of six different uncertainty sources on climate change impact projections of hydrology in a Canadian river basin. They calculated the mean annual hydrograph for each group to study the contributions of individual sources in overall uncertainty. They used a cumulative hydrograph derived from the mean hydrograph of each group and the cumulative distribution functions of 95% low flow and peak discharge. Yip et al. (2011), quantified the contribution of different uncertainty sources in the projection of surface air temperature using the analysis of variance (ANOVA) approach. The ANOVA approach has fewer assumptions as compared to other frequently used methods for uncertainty estimation, such as Recursive Model and Parameter Identification (e.g. Thiemann et al. 2001; Wagener et al. 2003), classical Bayesian approaches (e.g. Haydon and Deletic 2009; Kuczera et al. 2006), pseudo Bayesian methods such as GLUE (e.g. Beven and Binley 1992; Freni et al. 2009), and methods based on Frequentist Statistical Inference (Montanari 2007). The ANOVA approach can be used for uncertainty decomposition by determining deviations of each individual model projection from the ensemble mean of all projections (Deque et al. 2007; Yip et al. 2011). Further, Bosshard et al. (2013), improved the ANOVA method by proposing a sampling technique between different model projections to avoid biased variance decomposition in analyses of the uncertainty decomposition of large-scale watershed modeling.

Overall, examination of Table 1 reveals that: (1) using the ANOVA is comparatively recent method and there is an increasing interest in using this approach for uncertainty decomposition; (2) there is limited information on the effects of hydrologic model parameterization (HM-P) and regionalization (HM-R) scheme in the cascade of climate change uncertainty prediction, while the effects of hydrological model structure (HM-S) on overall uncertainty has been well considered in literature; and (3) there is spatiotemporal

Table 1 Summary of published studies that investigated the contribution of different sources of uncertainty into the overall cascade of uncertainty in climate-impact projections

Study	Sources of uncertainty								Interaction of sources	Uncertainty decomposition	Variables	Findings
	GCMs-S	GCMs-ic	GGES	SDS	DDS (RCM)	HM-S	HM-R	HM-P				The share of each uncertainty sources (major to minor)
Wilby and Harris (2006)	4		2	2		2		2	No	No	River low flow	GCM, DS, HM-P, GGES
Key et al. (2009)	5	3	1	1	8	2			No	No	Peak flow, Flood frequency	*Case 1*: GCM-ic, RCM, GCMs-S, HM-S, DS, GGES, HM_P *Case 2*: RCM, GGES, GCMs-S, GCMs-ic, DS, HM-P, HM-S
Prudhomme and Davies (2009)	3		2	1	3 (1)	2		10	No	No	River flow	GCM, DS, GGES, HM-P
Abbaspour et al. (2009) and Faramarzi et al. (2009)	1		3	1		1	506 sub-basin	400 to 500, 26 par	No	No	Precipitation, Temperature, BW, GWF & GWS	HM-P, HM-R, GGES
Chen et al. (2011a, b)	6	5	2	4		3			No	No	Annual, seasonal, & peak River flow	GCMs, DS, GCM-ic, GGES, HM-S, HM-P
Poulin et al. (2011)						2	Yes	1000, 23, 12 par	No	No	River flow, Soil water, Snow water equivalent	HM-S, HM-P
Yip et al. (2011)	7	2	3						Yes	Yes	Temperature	2010–2055: GCMs-S, GGES, GCMs-ic, Interaction 2056–2100: GGES, GCMs-S, GCMs-ic, Interaction
Harding et al. (2012)	16		3	1		1			No	No	River flow, Precipitation, Temperature	GCM, GGES, SDS, HM-S
Bosshard et al. (2013)	8			2		2			Yes	Yes	Temperature, Precipitation, River flow	*Summer and Fall*: GCM *Winter and Spring*: HM-S and DS and GCMs

Table 1 (continued)

Study	Sources of uncertainty								Interaction of sources	Uncertainty decomposition	Variables	Findings
	GCMs-S	GCMs-ic	GGES	SDS	DDS (RCM)	HM-S	HM-R	HM-P				The share of each uncertainty sources (major to minor)
Vetter et al. (2015)	5		4			3			Yes	Yes	River flow (low, mean, high)	Case 1: GCMs, GGES, HM-S, Interaction Case 2: GCMs, HM-S, GGES, Interaction Case 3: GGES, GCMs, Interaction, HM-S
Vetter et al. (2017)	5		4			9			Yes	Yes	River flow (low, mean, high)	GCMs, GGES, HM-S
Teklesadik et al. (2017)	4		4			9			No	No	River flow, ET (GWF)	GCMs-S, HM-S, GGES
This study	9		2	2	10	1	2255 sub-basin	1000 31 par	Yes	Yes	Precipitation, mean temperature, BW, GWF	CM, HM-P and HM-R, BCDS, ET methods, RCPs

variability on the order and share of different uncertainty sources. With this background, we devised a method to determine the contribution of HM-P and HM-R to the overall climate-impact uncertainty chain, and used this method to determine how spatial and temporal variation of hydro-climate conditions affect the uncertainty decomposition results. We have hypothesized that parameterization and regionalization of a hydrologic model may have a significant contribution in the cascade of uncertainty and its magnitude may outweigh other major sources of uncertainty in climate-impact projections.

To test our hypothesis, we used the previously calibrated-validated SWAT model of Alberta, Canada (Faramarzi et al. 2015, 2017) with the detailed model parameterization and regionalization at sub-basin level. This detailed model allows us to evaluate impacts of spatiotemporal hydro-climatic variability on the uncertainty decomposition results. We performed our analyses over two future periods including near future from 2010 to 2035, called S1, and far future from 2040 to 2065, called S2. We developed a compound approach consisting of the ANOVA method for decomposition of uncertainty sources and the SUFI-2 method for capturing the uncertainty associated with HM-P and HM-R in the overall uncertainty cascade of projected hydro-climatic variables. In addition to the HM-P and HM-R, we considered six other sources of uncertainty in this study namely: GCMs, RCPs, RCMs, bias correction and downscaling (BCDS) of climate data, and two different potential evapotranspiration (ET) calculation methods, i.e. Penman–Monteith and Hargreaves, which are widely-used approaches in hydrological models. We further quantified the share of each source of uncertainty and their interaction in the overall uncertainty. For this purpose, we quantified hydro-climate components including blue water availability (water yield plus deep aquifer recharge), green water flux (actual evapotranspiration), green water storage (soil moisture), precipitation, and mean temperature for two future horizons (i.e., 2010–2035 and 2040–2065). More information about the hydrological cycle of SWAT is presented in Figure SI.1 in Supplemental Information. For uncertainty decomposition, we aggregated the results from the sub-basin level to the provincial level.

2 Study area, data, and methods

2.1 Study area: Alberta, Canada

We tested our hypothesis using the province of Alberta as an example study area. Alberta with an area of about 660,000 km^2 has 17 large regional watersheds (Fig. 1), with considerable variability in hydro-climatic conditions, and each is projected to be highly influenced by future climate change (Masud et al. 2018). The watersheds principally originate from the east slopes of the Canadian Rockies and drain eastward to Hudson Bay through the provinces of Saskatchewan and Manitoba or northward to the Arctic Ocean. The province has relatively dry continental climate with warm summers and cold winters. Winter and summer temperatures vary from −25.1 to −9.6 °C and 8.7 to 18.5 °C, respectively, while long-term mean annual temperature ranges from 3.6 to 4.4 °C (Jiang et al. 2017). Summer temperature can rise up to 40 °C while the lowest winter temperature can drop down to − 54 °C (Faramarzi et al. 2017). Alberta's landscape follows a gradient from extensive lowlands, deeply incised valleys with a mean altitude of 170 m above sea level (m.a.s.l) in Wood Buffalo National Park in the northeast and peaking at an elevation of more than 3740 m.a.s.l in the Rocky Mountain along the southwestern border. This topographic variation, as well as the temporal variation in sea surface temperature of the Pacific Ocean, has a pronounced influence on the climate dynamics (Faramarzi et al. 2017). Average annual precipitation ranges from 300 mm year^{-1} in the southeast to 450 mm year^{-1} in the north, and increases from east to west, where it can reach 600 mm year^{-1} or more in the foothills of the Rocky Mountains. The average annual precipitation across the province is 510 mm year^{-1}. The south and east-central portions are prone to drought conditions, sometimes persisting for several years, although even these areas can also receive heavy precipitation and overland flooding (Faramarzi et al. 2017).

2.2 Input data and climate scenarios

2.2.1 Future global climate model data, bias correction, and downscaling technique

Although key components including ocean, atmosphere, and land surface of the earth and climate systems are represented in GCMs of the Fifth Assessment Report (IPCC 2013), they are at scales that even coarse topographic features such as mountain ranges or land–water interfaces that affect climate at the local scale are not resolved. These features have significant effects on the current climate and the responses of a region to climate change. Therefore, bias correction and downscaling of the GCM data are necessary before their use in regional impact analysis. Downscaling is a method to bridge the gap between coarse-scale GCMs (several ~ 100 km grids) to finer scales (~ 10 km grids). There are two distinct approaches to downscale GCM data including dynamic downscaling using a Regional Climate Model (RCM), and statistical downscaling using statistical relationships between local climate variables and GCM predictions (Chen et al. 2013). The performance of statistical bias correction methods to downscale meteorological variables from GCMs is reported to be satisfactory in different hydro-climatological studies (Chen et al. 2011a). In

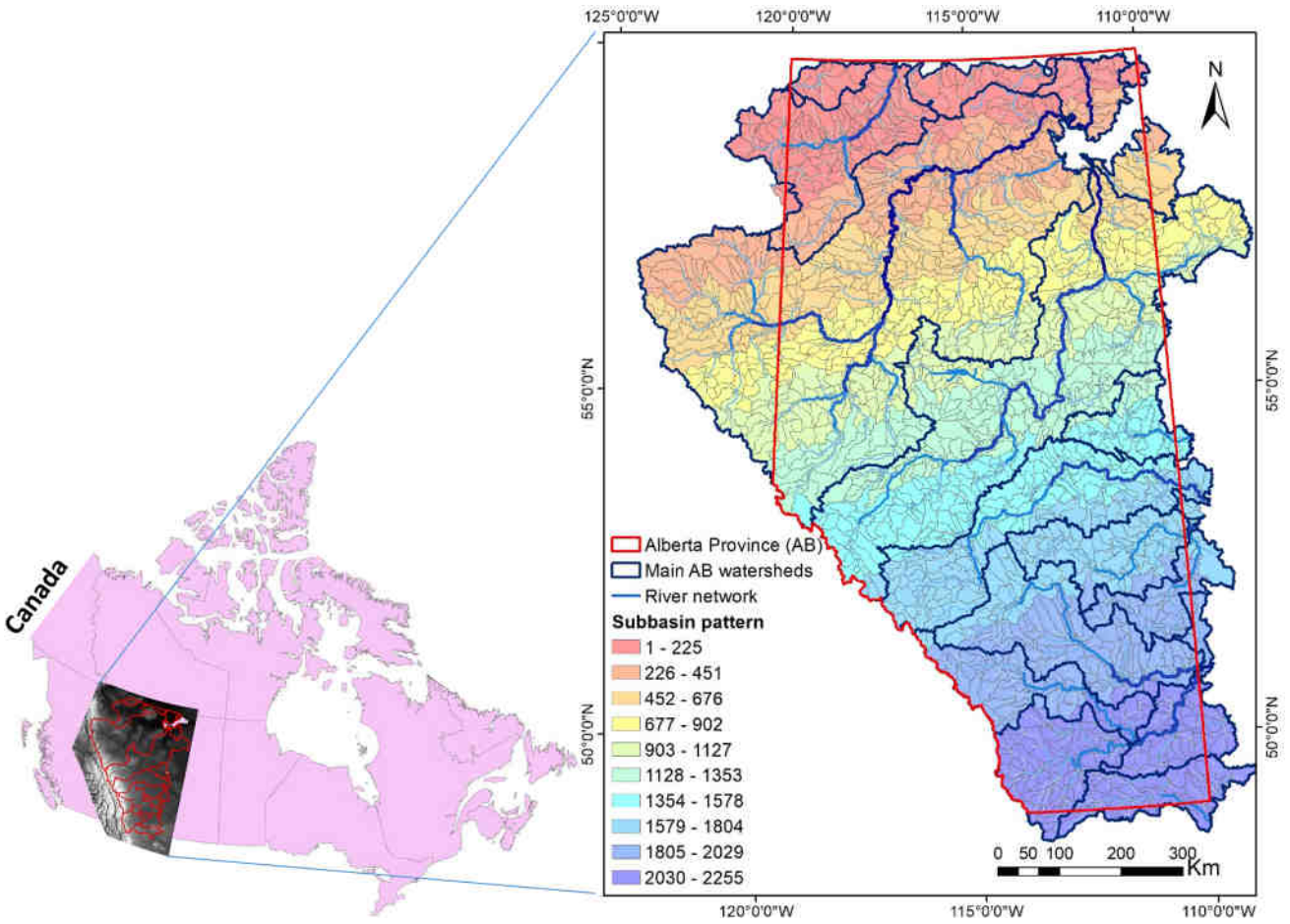

Fig. 1 Study Area including geographic extents, sub-basins pattern delineated through hydrologic model, river system and the 17 main watersheds originating from western highlands

this research, we examined two statistical bias correction approaches and dynamical downscaling, i.e. RCM in our analyses (see also Sect. 2.2.2). For statistical bias correction, we used the statistically downscaled data from the Pacific Climate Impacts Consortium (PCIC) with no additional bias correction (ND) to the local scale, i.e. Alberta. Secondly, we applied the delta change (Chen et al. 2011a) method (D) to PCIC data for further bias correction to represent Alberta climate conditions. There are various downscaling and bias correction methods available for climate change studies. The performance of these methods has been compared in the literature (Räty et al. 2014). The delta change method reflects the climate change signals of each GCM into an identical baseline scenario. The PCIC data used in this study included nine sets of GCMs (1980–2069), under two RCPs (Cannon 2015; PCIC 2014), using subsets of the Coupled Model Inter-Comparison Project (CMIP5). A description of the models is summarized in Table 2. Two selected RCP 2.6 (van Vuuren et al. 2011) and RCP 8.5 (Riahi et al. 2011), properly represent a large range of uncertainty. RCP 2.6 describes the best case for limiting anthropogenic climate change, while in RCP 8.5 carbon emissions rapidly increase by the end of the century. A total number of 2150 grid-points were located in the study area based on the available data at a gridded resolution of roughly 10 km. Selected GCMs cover most of the possible uncertainty range of available IPCC models and provide the widest spread in the future climate (Cannon 2015). GCMs structure and spatial resolution are other uncertainty sources that contribute to the overall uncertainty of climate projection.

2.2.2 Future regional climate model data and initial condition

A suite of ten RCMs driven from an ensemble of atmosphere–ocean general circulation models (AOGCMs) over a domain of North America, covering the United States and most of Canada, are considered in this study. These data are available through the North American Regional Climate Change Assessment Program (NARCCAP). Table 3,

Table 2 General information of selected GCMs and scenarios available from PCIC

Acronym	Country	Resolution	Scenario
CanESM2	Canada	Canadian Centre for Climate Modeling and Analysis	RCPs 2.6, 8.5
CCSM4	United States	National Center for Atmospheric Research	RCPs 2.6, 8.5
CNRM-CM5	France	Centre National de Recherches Meteorologiques/Centre Europeen de Recherche et Formation Avancees en Calcul Scientifique	RCPs 2.6, 8.5
CSIRO-MK3.6.0	Australia	Commonwealth Scientific and Industrial Research Organization in collaboration with the Queensland Climate Change Centre of Excellence	RCPs 2.6, 8.5
GFDL-ESM2G	United States	Geophysical Fluid Dynamics Laboratory	RCPs 2.6, 8.5
HadGEM2	United Kingdom	Met Office Hadley Centre (additional HadGEM2-ES runs by Instituto Nacional de Pesquisas Espaciais)	RCPs 2.6, 8.5
MIROC5	Japan	Meteorological Research Institute	RCPs 2.6, 8.5
MPI-ESM-LR	Germany	Max Planck Institute for Meteorology	RCPs 2.6, 8.5
MRI-CGCM3	Japan	Meteorological Research Institute	RCPs 2.6, 8.5

Table 3 The NARCCAP regional climate models used in this study

RCM	Driving GCM					Acronym for each model
	CESM2	CCSM	CGCM3	GFDL	HadCM3	
CRCM	✓	✓	✓			CRCM-CESM2 CRCM-CCSM CRCM-CGCM3
ECP2				✓		ECP2-GFDL
HRM3				✓	✓	HRM3-GFDL HRM3-HadCM3
MM5I		✓			✓	MM5I-CCSM MM5I-HadCM3
RCM3			✓	✓		RCM3-CGCM3 RCM3-GFDL

summarizes the RCMs (Mearns 2014) that were used in this study. In NARCCAP, the RCMs simulations were produced in two phases. In the first phase, simulations from various regional models, i.e. CRCM, ECP2, HRM3, MM5I, RCM3 and WRFG RCMs were produced according to boundary conditions from National Centers for Environmental Prediction (NCEP) reanalysis II for 1981–2003 reference period (Mearns et al. 2009). In the second Phase, RCM simulations (~ 50 km grids) for the 1970–1999 period and 2041–2070 future scenarios were produced using the boundary conditions of different GCMs (i.e. CCSM, CGCM3, GFDL, and HADCM3), and the Special Report on Emission Scenarios (SRES) A2 of the CMIP3 emission scenario (Nakicenovic et al. 2000). We used the RCMs to examine two hydrologic model scenarios based on two potential evapotranspiration calculation methods: (1) Hargreaves (Hargreaves et al. 1985) method, which is based on precipitation and temperature time series; and (2) Penman–Monteith (Penman 1948), which requires relative humidity, solar radiation, and wind speed as well as precipitation and temperature time series. A total of 320 climate grid-points were located in the study area based on the available data at a gridded resolution of roughly 50 km.

2.3 Hydrological model

The hydrologic model of choice for this study was SWAT (Arnold et al. 1998, 2012). SWAT is a continuous time, semi-physically based, semi-distributed, agro-hydrologic model running on daily time steps (See Figure SI.1 of the Supplemental Information for the schematic hydrological cycle in SWAT). The model has been developed to quantify the impacts of climate change and land management practices on water, sediment, and agricultural chemical yields in large complex watersheds with varying soils, landuse, and management conditions over long periods of time. The program, therefore, lends itself easily to climate and landuse change analyses. A more detailed description of the SWAT model is provided in Arnold et al. (2012). We used the SWAT model of Alberta that had already been set up, calibrated and validated for the period of 1983–2007 (Faramarzi et al. 2017, 2015) using the SUFI-2 algorithm of SWAT-CUP (Abbaspour et al. 2007, 2017). The authors parameterized the SWAT model using a total of 31 sensitive input parameters (i.e. SCS runoff curve number for moisture condition II, base flow alpha factor, etc.) over 2255 subbasins (Fig. 1). A regionalization approach was applied to

further differentiate the physical parameters based on hydro-climatic conditions in 17 main river basins in Alberta. This resulted in a total of over 1000 physical parameters being altered throughout the study area by using a regionalized parameterization, calibration, and validation scheme (Faramarzi et al. 2015, 2017).

2.4 Model setup, experimental frameworks, and uncertainty decomposition

2.4.1 Model setup

We chose the 1983–2007 period as the reference (historical period) and selected 2010–2035 (near future, S1) and 2040–2065 (far future, S2) periods for future analyses. We evaluated the projections of five hydro-climate variables namely precipitation, mean temperature, blue water availability (which is water yield plus deep aquifer recharge), green water storage (soil moisture), and green water flow or actual evapotranspiration (Falkenmark and Rockström 2006). Under each climate model and RCP trajectory, we performed 1000 hydrologic model simulations with altering input parameters that resulted in 1000 projections for each hydro-climate variables. Further, we calculated three quantiles for each of the variables and used in decomposition analyses, representing high ($Q_{97.5}$), low ($Q_{2.5}$), and the median (Q_{50}) conditions in the HM-P and HM-R projections. Later, we used these quantiles and developed the ANOVA-SUFI-2 method, to decompose the overall uncertainty into each driver's share (see Sect. 2.4.2). To analyze the level of agreement or discrepancy among climate models and RCP trajectories, we used the coefficient of variation (CV) which expresses the degree of reliability in the projection of variables over time. Covering all possible future climate-impact projections based on the available input data, and proper implementation of the ANOVA-SUFI-2 method, we set up 92 SWAT-CUP projects under two frameworks and three scenario-sets, which we describe in more details in the next section and in Supplemental Information, section SI.1.

2.4.2 Uncertainty evaluation and decomposition

We used a combination of analysis of variance method -ANOVA- (Deque et al. 2007; von Storch and Zwiers 1999; Yip et al. 2011) and SUFI-2 program for evaluation of different sources of uncertainty in the projected hydrological changes of Alberta. ANOVA is used to assess the contribution of different sources of uncertainty to the total predicted uncertainty of the projected variables. Using ANOVA, the variances in the projected changes are split into the original contributing sources and the interaction of different sources with each other. The interaction of different sources shows the share of uncertainty sources that do not behave linearly. For instance, the snow melt parameters of the hydrologic model are affected by temperature projections of climate models, and could lead to nonlinear runoff responses (Bosshard et al. 2013). This can be quantified through an interaction component of the ANOVA decomposition approach. The SUFI-2 algorithm is used to map all 'hydrologic' model uncertainties (i.e. parameter, conceptual model, input data, model structure) on the hydrologic model parameter ranges, and captures the measured data within the 95% prediction uncertainty range (95PPU) which is calculated at the 2.5% and 97.5% levels of the cumulative distribution of an output variable obtained through Latin Hypercube Sampling (McKay et al. 1979, 2000). The combination of ANOVA and SUFI-2 methods thereby accounts for combined HM-P and HM-R in the decomposition of ensemble uncertainty in climate change projections. Overall, potential sources of uncertainty for our decomposition analysis were related to RCPs, GCMs, RCMs, BCDS, ET calculation methods, and HM-P and HM-R originated from the 92 experiments performed under the two frameworks (Fig. 2). In framework-1, we used a three-factor ANOVA for uncertainty analysis of projected changes in blue and green water components due to different GCMs, RCPs, and BCDS. In framework-2, we implemented a two-factor ANOVA incorporating different RCMs, and potential evapotranspiration calculation methods. The cascade of uncertainty used in these two frameworks is presented in Fig. 2 (for those who are less familiar with the ANOVA approach, we recommend they first read the framework 2 structure). In the framework-1, the total sum of square errors (*SST*) is defined as:

$$\mathrm{SST} = \sum_{i=1}^{N_{RCP}} \sum_{j=1}^{N_{GCM}} \sum_{k=1}^{N_{BCSD}} (X_{ijk} - \bar{X}_{ooo})^2 \tag{1}$$

where, X_{ijk} is the value of hydro-climate variable X (in this study differences of future and historical blue and green water components) corresponding to RCP i, GCM j, and BCDS k, respectively, and $\bar{X}_{ooo}$ is the overall mean. To investigate the contribution of HM-P and HM-R to the overall uncertainty, we used the 2.5, 50, and 97.5 quantiles out of 1000 SWAT runs for the projected hydrological variables (blue and green water), which represent low, medium, and high conditions, respectively. We computed quantiles in each model time-series and then averaged over the ensemble. We adjusted the above formula in Eq. 2 by considering three quantiles ($Q_{2.5}$, Q_{50}, $Q_{97.5}$) of variable X derived from 1000 simulations of the SWAT model at 95% confidence level.

$$\mathrm{SST} = \sum_{i=1}^{N_{RCP}} \sum_{j=1}^{N_{GCM}} \sum_{k=1}^{N_{BCSD}} (QX_{ijk} - \overline{QX}_{ooo})^2 \tag{2}$$

where, QX_{ijk} and $\overline{QX}_{ooo}$ are the three quantiles ($Q_{2.5}$, Q_{50}, $Q_{97.5}$) of X_{ijk} and $\bar{X}_{ooo}$, respectively. In this study,

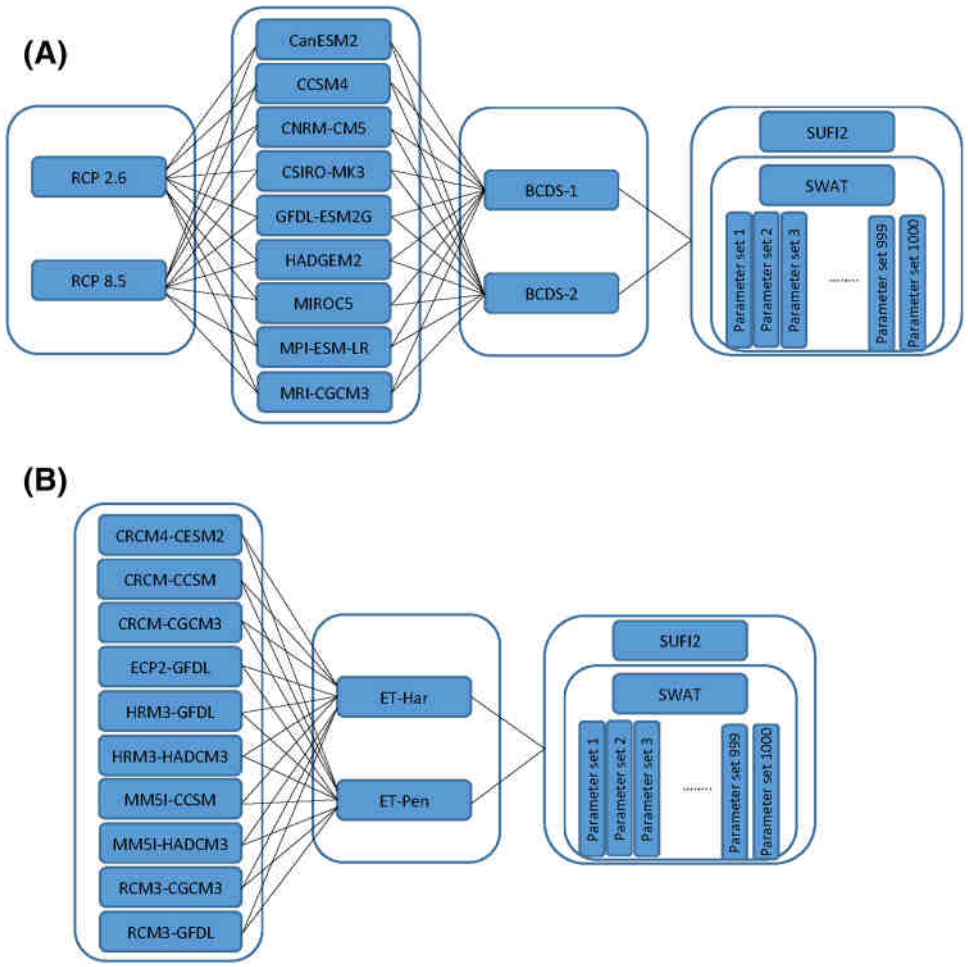

Fig. 2 Uncertainty cascade frameworks developed for the study purposes

1000 SWAT runs were performed based on (1) the minimum suggested number of SWAT runs in the literature for a proper uncertainty analysis (Abbaspour et al. 2015); (2) the number of sub-basins in SWAT model of Alberta, i.e. 2255 (Faramarzi et al. 2015); and (3) the sensitive parameters in uncertainty analysis (31 variables regionalized for the 17 river basins, see Table SI.2 in Supplemental Information for more details).

Based on the ANOVA theory, SST can be divided into the sum of squares of errors due to individual effects and their interactions:

$$\mathrm{SST} = SS_{RCP} + SS_{GCM} + SS_{BCDS} + \mathrm{SSI} \tag{3}$$

$$\mathrm{SSI} = SS_{RCP*GCM} + SS_{RCP*BCDS} + SS_{GCM*BCDS} + SS_{RCP*GCM*BCDS} \tag{4}$$

$$\mathrm{SS}_{RCP} = N_{GCM}N_{BCDS}\sum_{i=1}^{N_{RCP}}(\overline{QX}_{ioo} - \overline{QX}_{ooo})^2 \tag{5}$$

$$\mathrm{SS}_{GCM} = N_{RCP}N_{BCDS}\sum_{j=1}^{N_{GCM}}(\overline{QX}_{ojo} - \overline{QX}_{ooo})^2 \tag{6}$$

$$SS_{BCSD} = N_{RCP}N_{GCM}\sum_{k=1}^{N_{BCDS}}(\overline{QX}_{ook} - \overline{QX}_{ooo})^2 \tag{7}$$

$$SSI = \sum_{i=1}^{N_{RCP}}\sum_{j=1}^{N_{GCM}}\sum_{k=1}^{N_{BCDS}}(QX_{ijk} - \overline{QX}_{ioo} - \overline{QX}_{ojo} - \overline{QX}_{ook} + 2\overline{QX}_{ooo})^2 \tag{8}$$

where, N_{RCP}, N_{GCM}, and N_{BCDS} describe the number of RCPs, the number of GCMs and the number of bias correction statistical downscaling methods, respectively. The symbol "$_{o}$" indicates averaging over a particular index.

In ANOVA, unequal population size of different uncertainty sources (in our study: GCMs population size = 9, RCPs population size = 2 and BCDS population size = 2) may cause bias in the uncertainty decomposition results (Bosshard et al. 2013). To avoid the bias caused by different population sizes of GCM sources, we followed the approach of Bosshard et al. (2013), sampling all the possible combinations of selecting two of nine GCMs $\left(\binom{9}{2} = 36\right)$, two of two RCPs $\left(\binom{2}{2} = 1\right)$, and two of two BCDS $\left(\binom{2}{2} = 1\right)$. The sam-

pling procedure resulted in total of 36 possible sample sets ($36 \times 1 \times 1 = 36$) for framework-1, each sample set included two RCPs, two GCMs, and two BCDS (a total of $2 \times 2 \times 2 = 8$ combinations). Next, we calculated all the terms of SST in Eq. 3 (i.e. Eqs. 5–8) for each of the 36 sample sets that resulted in a total of 36 $SS_{RCP,}$ 36 $SS_{BCD,}$ 36 SS_{GCM}, and 36 SSI. Further, we aggregated them to account for 'unbiased variance fraction' ($NSST_U$) by using Eq. 9 (Bosshard et al. 2013) to obtain the final SS_{RCP}, SS_{BCDS}, SS_{GCM} and SSI:

$$NSS_U = \frac{1}{36} \sum_{m=1}^{36} \frac{SS_{U,m}}{SST} \tag{9}$$

where, $_U$ indicates the uncertainty component, i.e. RCP, GCM, BCDS, and SSI. Therefore, a total of four variance fractions were calculated, including of NSS_{RCP}, NSS_{GCM}, NSS_{BCDS}, $NSSI$.

In order to study the uncertainty associated with the climate change, the systematic model bias in climate model projections has to be removed first. Two common approaches to omit such discrepancies are (1) using a Delta method (Kay et al. 2009) and force the historical simulations of GCMs to follow the historically observed climate, so that all historical simulations of GCMs would be identical, and (2) considering differences between historical and future simulations of the same modeling chain, after the entire chain of models has been executed (i.e. subtract the result of the historical simulation from the result of the future simulation, and only consider the changes). In this study, the second approach which uses the differences between historical and future simulations of blue and green water instead of absolute values of future simulations, considered to be more suitable, since it allows for more flexibility in bias-correction.

Likewise, in the framework-2, the total sum of squares (SST) is defined as:

$$\mathrm{SST} = \sum_{i=1}^{N_{RCM}} \sum_{j=1}^{N_{ET}} (QY_{ij} - \overline{QY}_{oo})^2 \tag{10}$$

where QY_{ij} and $\overline{QY}_{oo}$ are three quantiles ($Q_{2.5}$, Q_{50}, $Q_{97.5}$) of Y_{ij} and $\bar{Y}_{oo}$ respectively, and Y_{ij} is the value of hydro-climate variable Y corresponding to RCM i, and potential evapotranspiration calculation method j. $\bar{Y}_{oo}$ is the overall mean.

SST is split into the sum of squares due to individual effects and their interactions:

$$\mathrm{SST} = SS_{RCM} + SS_{ET} + \mathrm{SSI} \tag{11}$$

$$SSI = SS_{RCM*ET} \tag{12}$$

$$\mathrm{SS}_{RCM} = N_{ET} \sum_{i=1}^{N_{RCM}} (\overline{QY}_{io} - \overline{QY}_{oo})^2 \tag{13}$$

$$\mathrm{SS}_{ET} = N_{RCM} \sum_{j=1}^{N_{ET}} (\overline{QY}_{oj} - \overline{QY}_{oo})^2 \tag{14}$$

$$\mathrm{SSI} = \sum_{i=1}^{N_{RCM}} \sum_{j=1}^{N_{ET}} (QY_{ij} - \overline{QX}_{io} - \overline{QY}_{oj} + \overline{QY}_{oo})^2 \tag{15}$$

where, N_{RCM}, and N_{ET} describe the number of RCMs, and the number of ET calculation methods respectively. The symbol "o" indicates averaging over a particular index.

For framework-2 a total of ten RCMs and two ET calculation methods were sampled based on the Bosshard et al. (2013) approach. Therefore, all possible combination of two of ten RCMs $\left(\binom{10}{2} = 45\right)$, and two of two ET $\left(\binom{2}{2} = 1\right)$ methods were covered. For framework-2, each sample set included two RCMs, two ETs methods (a total of 4 combinations). Thus, we attained a total of 45 subsamples. After calculation of all the terms of SST in Eq. 11 for all 45 samples, the unbiased variance fraction related to different components were quantified as:

$$NSS_U = \frac{1}{45} \sum_{m=1}^{45} \frac{SS_{U,m}}{SST} \tag{16}$$

where, $_U$ indicates the uncertainty component, i.e. RCM, ET calculation methods, and SSI. Therefore, a total of three variance fractions were calculated, including of NSS_{RCM}, NSS_{BET}, $NSSI$.

For the framework-2, we implemented the ANOVA-SUFI-2 analysis on both absolute values of future simulations of ten RCMs, and differences of future and historical simulations of seven RCMs (i.e., using median, upper, and lower bound quantiles of projected precipitation and temperature from ensemble of RCMs). We presented results of the first implementation in Sect. 3.2, and illustrated results of the second implementation in the Supplemental Information (Figure SI.5).

As mentioned in earlier sections, we setup 92 SWAT-CUP project experiments based on the uncertainty analysis frameworks and different uncertainty sources considered in this study (Fig. 2; Table 4). To present the analyses, we categorized all 92 possible model experiments into three scenario-sets, as demonstrated in Table 5. After running all scenarios, we implemented the ANOVA analysis for each framework and scenario-set to calculate the share of different sources of uncertainty for changes in blue and green water components.

To prepare each of the 92 SWAT-CUP projects and conduct the experiments, we provide a step-wise guideline,

Table 4 Climate–Impact scenarios used in this study

Scenarios	Description	Acronym
	Historical, 1983–2007	Historical
Sc 1–9	9 GCMs, RCP 2.6, downscaled, 2010–2035	GCM-RCP 2.6-D-S1
Sc 10–18	9 GCMs, RCP 2.6, downscaled, 2040–2065	GCM-RCP 2.6-D-S2
Sc 19–27	9 GCMs, RCP 2.6, not downscaled, 2010–2035	GCM-RCP 2.6-ND-S1
Sc 28–36	9 GCMs, RCP 2.6, not downscaled, 2040–2065	GCM-RCP 2.6-ND-S2
Sc 37–45	9 GCMs, RCP 8.5, downscaled, 2010–2035	GCM-RCP 8.5-D-S1
Sc 46–54	9 GCMs, RCP 8.5, downscaled, 2040–2065	GCM-RCP 8.5-D-S2
Sc 55–63	9 GCMs, RCP 8.5, not downscaled, 2010–2035	GCM-RCP 8.5-ND-S1
Sc 64–72	9 GCMs, RCP 8.5, not downscaled, 2040–2065	GCM-RCP 8.5-ND-S2
Sc 73–82	10 RCMs, 2040–2065, Hargreaves	RCM-Har-D-S2
Sc 83–92	10 RCMs, 2040–2065, Penman–Monteith	RCM-Pen-D-S2

Table 5 Frameworks and scenario combinations used for assessment of uncertainty cascade

Scenarios	Scenario-set
GCMs-RCP 2.6-D-S1	Scenario-set1 (GCMs-2010-2035)
GCMs-RCP 2.6-ND-S1	
GCMs-RCP 8.5-D-S1	
GCMs-RCP 8.5-ND-S1	
GCMs-RCP 2.6-D-S2	Scenario-set2 (GCMs-2040-2065)
GCMs-RCP 2.6-ND-S2	
GCMs-RCP 8.5-D-S2	
GCMs-RCP 8.5-ND-S2	
RCMs-Har-D-S2	Scenario-set3 (RCMs-2040-2065)
RCMs-Pen-D-S2	

which can be used as a protocol in any climate change study using the SWAT model (see Supplemental Information, section SI.2 for the protocol of climate change study with SWAT).

3 Results and discussion

3.1 Hydro-climatic impacts

For the sake of brevity, we only report the results of our analyses at the 50% quantile level, in Sect. 3.1.1–3.1.4 (Figs. 3, 4, 5, 6, 7). We present ensemble results of BCDS for nine GCMs and two RCPs, and ensemble results of ten RCMs for two ET calculation methods. To avoid inconsistency in the results, we eliminated the two extreme outliers of each scenario set in the results of CVs and SDs. To better interpret the impacts of climate change on water resources under different scenarios, we compared the results of future with historical simulations in Sect. 3.1.1 to 3.15. Table SI.3 summarizes the statistics of spatial variation of projected changes and CVs of precipitation, average temperature, blue water, and green water resources (see Supplemental Information). The decomposition of uncertainty is performed using all three quantiles and the results are presented in Sects. 3.2 and 3.3.

3.1.1 Precipitation trends

Figure 3 shows the historical long-term average annual precipitation obtained through previous studies of Alberta (Faramarzi et al. 2015, 2017), and projected differences between future and historical precipitation scenarios. The historical distribution of annual precipitation (Fig. 3a) ranges from 280 mm year^{-1} in the southeast to 750 mm year^{-1} in the Rocky Mountains (see Figure SI.2 in Supplemental Information for seasonal distribution precipitation across Alberta). The median of the results from an ensemble of 9 downscaled GCM-RCP runs for the 2010–2035 horizon (Fig. 3b, d) showed that most of the study area will experience a likely increase of 0 to 5% in precipitation (i.e. 0 to 50 mm year^{-1}) with an average of 16 and 10 mm year^{-1} across the province under RCP2.6 and 8.5 scenarios, respectively (Table SI.3). The results (Fig. 3c, e) showed relatively larger rise for the 2040–2065 (GCMs-RCP2.6-D-S2 and GCMs-RCP 8.5-D-S2) period as compared to the 2010–2035 period, with a likely increase of 5–20% (i.e. 20 to 60 mm year^{-1}). Meanwhile, the province's average increase of 32 and 36 mm year^{-1} under RCP2.6 and 8.5 was projected, respectively (Table SI.3). Figure 3f presents projected changes in precipitation for 2040–2065 horizon using the median of the results from an ensemble of ten RCM runs. The magnitude of the changes strongly increased from GCMs to RCMs with more increases in the western part of the province. The long-term average annual precipitation changes over the province showed a likely increase of 117 mm year^{-1} (Table SI.3). The RCMs projections of 15–20% increases for precipitation agree with the previous studies (Erler and Peltier 2017; Jeong et al. 2014; Mearns et al. 2013). Figure 3g–k show the coefficient of variations (CVs) of the climate model

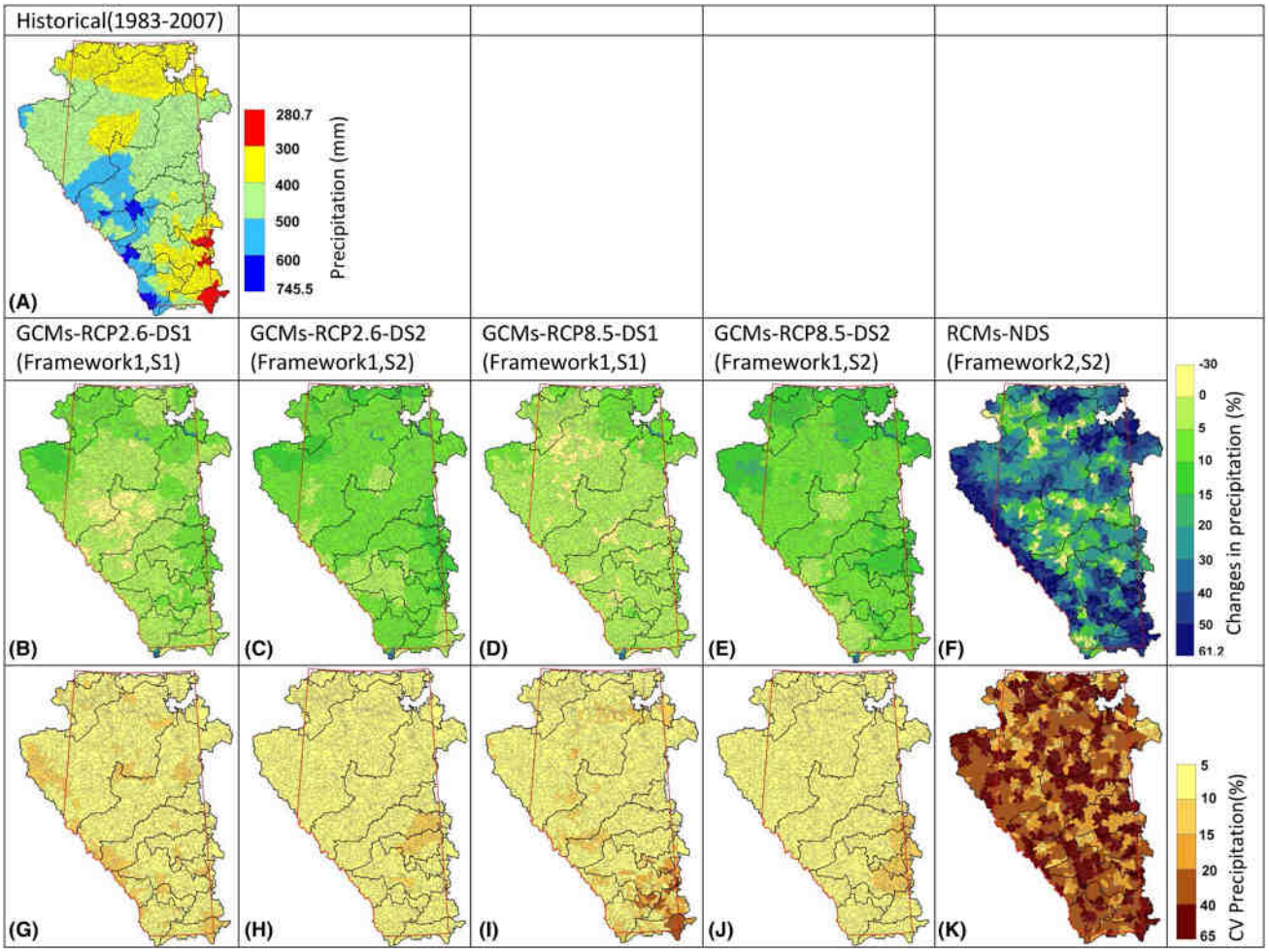

Fig. 3 Spatial distribution of annual precipitation for historical period (1983–2007) (**a**), its changes (Changes = [[future values − historical values]/historical values] × 100) between near future (2010–2035) and historical period (**b, d**), and between far future (2040–2065) and historical period (**c, e**) calculated using ensemble of GCMs-bias corrected data under RCP 2.6 and RCP 8.5 scenarios, respectively. **f** The spatial distribution of changes between 2040 and 2065 and historical period calculated using the ensemble of RCMs. The coefficient of variation, indicating inter-model variation, for the near future (**g, i**), far future (**h, j**) under the RCP 2.6 and RCP 8.5 scenarios, respectively. **k** The coefficient of variation for RCM models projections

predictions. The smaller the CV, the less model-to-model variability of precipitation and more reliable are the predictions. A provincial average CV of 7.4% under RCP 2.6 and 8.5 indicated the same magnitude of consistency between models in projection of precipitation under the 2040–2065 future scenarios (Fig. 3h, j) as compared to the 2010–2035 scenarios (Fig. 3g, i), where a slightly larger average CV of 9% and 8% were found for RCP 2.6 and 8.5, respectively. For the 2040–2065 period, most of Alberta has small CVs of up to 10% (Fig. 3h, j), except the southeast region (Fig. 3j), where CVs of up to 20% were found for the 8.5 scenario. Our analysis showed an increase of up to 63% in precipitation under RCM scenarios with an average CV of 31% across the province. Stronger changes for precipitation in NARCCAP data compared to GCMs have been reported by other researchers as well (e.g. Erler and Peltier 2017; Mearns et al. 2013). A likely reason for higher agreement between historical and future data in GCM precipitation compared to RCM results of NARCCAP is the further bias-correction, which we applied to the GCM data (Laflamme et al. 2016). Furthermore, the RCM simulations may also present biases due to regional physical processes involved in these simulations, intensifying those from the driving GCM leading to a large combined error and disagreement among models (Fan et al. 2015; Gao et al. 2016).

3.1.2 Temperature trends

Figure 4 shows the spatial distribution of the long-term average annual temperature, i.e. mean temperature, for the reference period (1983–2007) and the differences between historical and future scenarios (2010–2035 and 2040–2065). In the

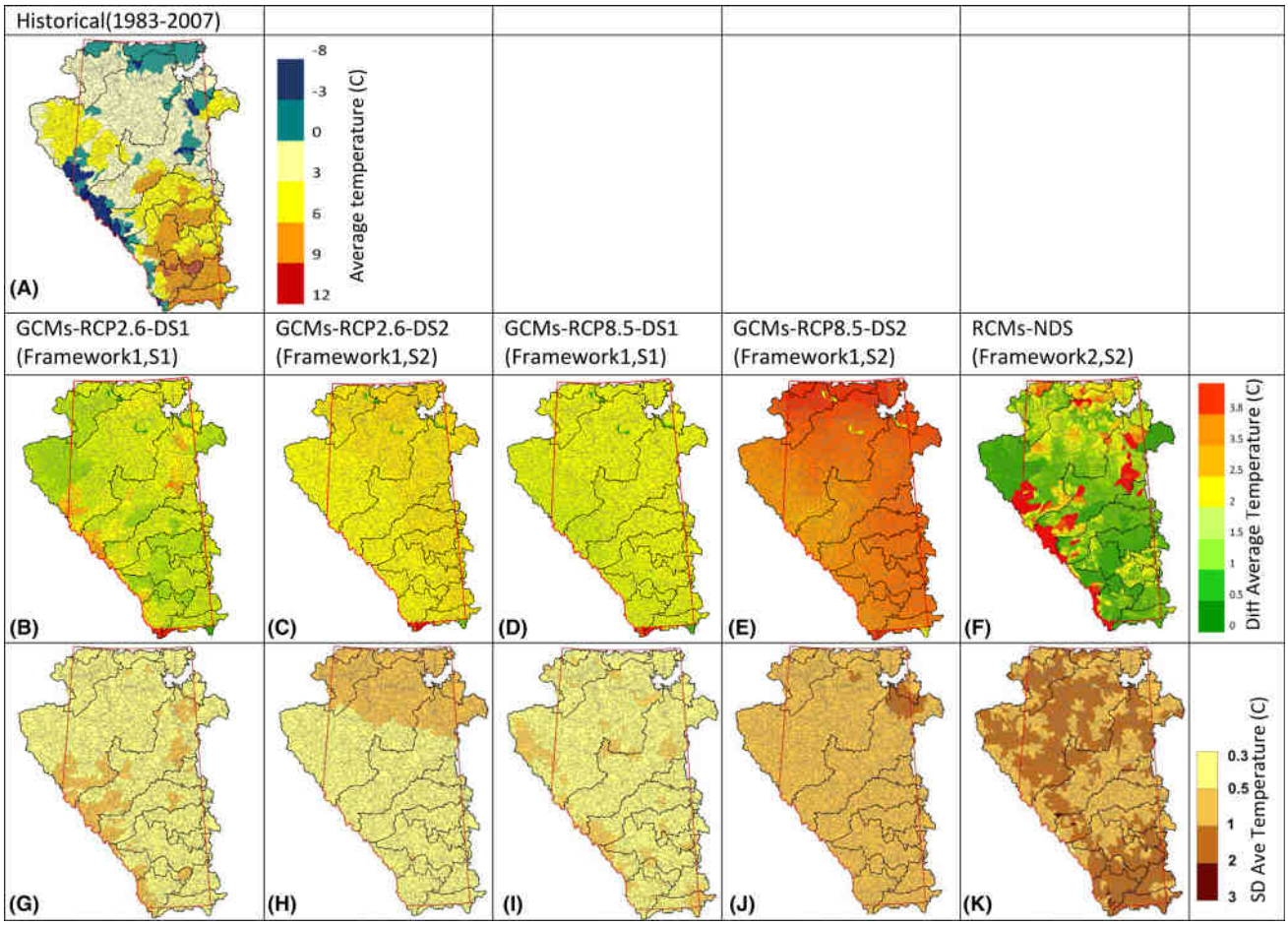

Fig. 4 Spatial distribution of annual mean temperature for historical period (1983–2007) (**a**), its changes (Changes = [[future values − historical values]/historical values] × 100) between near future (2010–2035) and historical period (**b, d**), and between far future (2040–2065) and historical period (**c, e**) calculated using ensemble of GCMs-bias corrected data under RCP 2.6 and RCP 8.5 scenarios, respectively. **f** The spatial distribution of changes between 2040 and 2065 and historical period calculated using ensemble of RCMs. The coefficient of variation, indicating inter-model variation, for the near future (**g, i**), far future (**h, j**) under the RCP 2.6 and RCP 8.5 scenarios, respectively. **k** The coefficient of variation for RCM models projections

near future, average increases of 1.35 °C under RCP 2.6 and 1.4 °C under RCP 8.5 were found for the province as a whole, while increases of up to 1.7 and 1.8 °C were found in various regions under RCP2.6 and 8.5, respectively (Fig. 4b, d). Furthermore, projections showed that some parts of Alberta will experience a warmer temperature of up to 3.8 °C in the far future (Fig. 4c, e) as compared to the near future. Overall, the far future increases are significantly higher under RCP8.5 (3 °C) compared to RCP2.6 (1.7 °C) across Alberta. The ensemble results of RCMs showed that the changes in mean temperature relative to the historical period vary between 0 °C in northwest and 2 °C in the Rocky Mountains, with an average increase of 1.7 °C and standard deviation (SD) of 1.3 °C across the province. Overall, our results showed a significantly higher spatial variation in RCMs as compared to GCMs for the reasons we mentioned in the earlier section and also the likely inconsistency in the physical representation of the climate system between RCMs and GCMs (Fernández et al. 2018; Roop et al. 2015). The long-term average SD of mean annual temperature for near future showed a slightly larger inter model disagreement (of up to 0.5 °C) in RCP 2.6 compared to 8.5 (of up to 0.4 °C) scenarios (Fig. 4g, i). Overall, the far future scenario results showed a low (0.3–0.5 °C) to moderate (0.5–1 °C) SD for the RCPs and GCMs in projection of mean temperature (Fig. 4h, j). Figure 4k displays disagreement (with an average of 2.36 °C) among RCMs for all sub-basins in the province. The large differences between individual NARCCAP RCM projections have also been previously reported (e.g. Jiang et al. 2016; Salazar et al. 2016).

3.1.3 Blue water

Figure 5 shows the spatial distribution of the annual blue water resources for the historical period (1983–2007) and

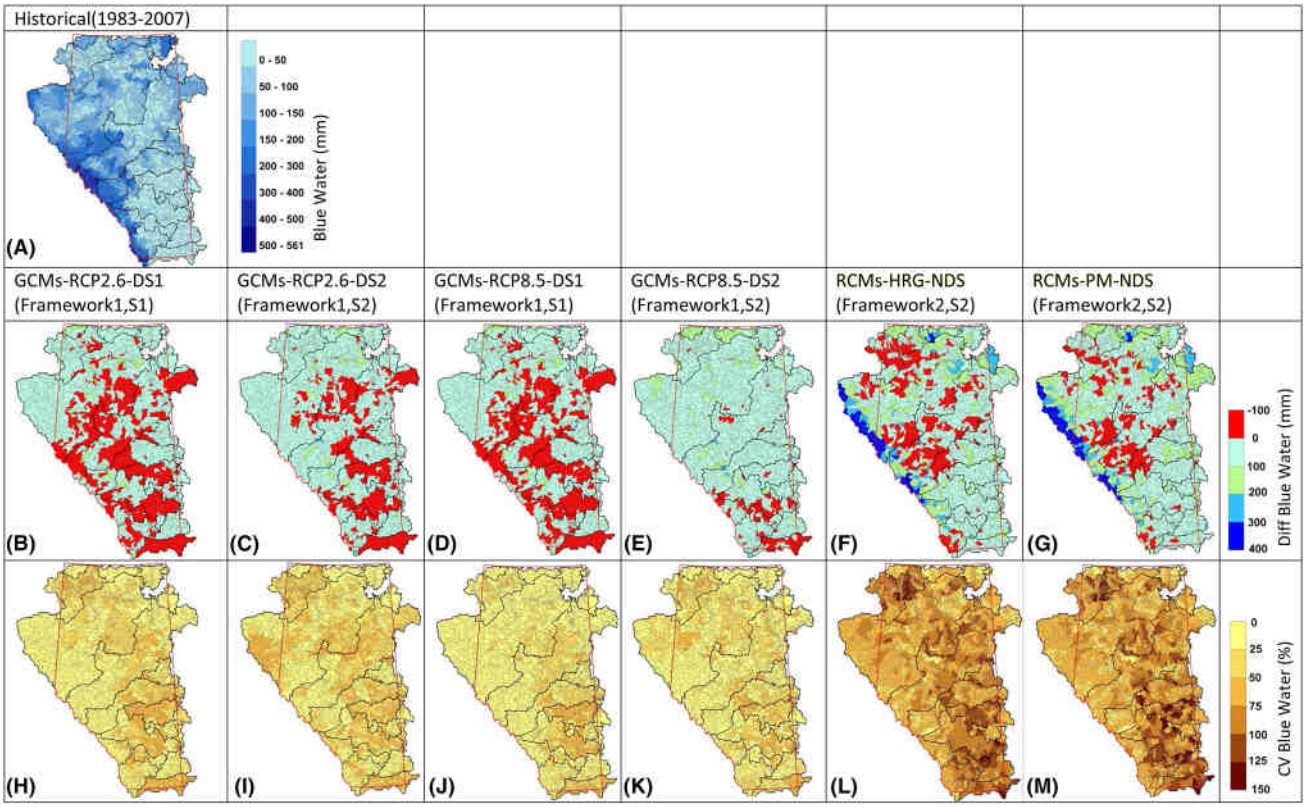

Fig. 5 Spatial distribution of annual blue water for historical period (1983–2007) (**a**), its changes (Changes = [[future values − historical values]/historical values] × 100) between near future (2010–2035) and historical period (**b, d**), and between far future (2040–2065) and historical period (**c, e**) calculated using ensemble of GCMs-bias corrected data under RCP 2.6 and RCP 8.5 scenarios, respectively. **f, g** The spatial distribution of changes between 2040 and 2065 and historical period calculated using ensemble of RCMs using Hargreaves and Penman Monteith evapotranspiration calculation methods respectively. The coefficient of variation, indicating inter-model variation, for the near future (**h, j**), far future (**i, k**) under the RCP 2.6 and RCP 8.5 scenarios, respectively. **l, m** The coefficient of variation for RCM models projections using Hargreaves and Penman–Monteith evapotranspiration calculation methods respectively

the changes in future scenarios (2010–2035 and 2040–2065). Historically, the annual blue water varied spatially from 10 to 561 mm, with highest values in the west and southwest and the lowest in the grasslands in the southeast of the province (Fig. 5a). Generally, the blue water was projected to increase in the north and north-west of the province in all GCMs by up to 100 mm (Fig. 5b–d). Blue water decreased in some sub-basins in the west, south, and central parts of the province, with an average of − 20, − 28, and − 27 mm year^{-1} in RCP 2.6-D-S1, RCP 2.6-D-S2, and RCP 8.5-D-S1, respectively (Fig. 5b–d). Blue water increased in RCP 8.5-D-S2 in most sub-basins with an average amount of 46 mm which is consistent with the precipitation increase in this scenario-set (Fig. 5e). Our results indicated that the blue water availability differs significantly in response to RCMs as compared to the GCMs; although there is a similar spatial pattern in both GCMs and RCMs. The magnitude of increase is much higher for RCMs scenarios, where for some western sub-basin an increase of up to 350 mm is seen (Fig. 5f, g) due to increasing precipitation in the RCMs (Fig. 3). The CV of GCMs (Fig. 5h–k) indicated larger agreement (0–50%) between GCMs. Slightly higher CV was found in far future scenarios (Fig. 5i, k) in comparison to the near future scenarios (Fig. 5h, j). In RCM model-scenarios higher discrepancy among RCMs was found for most of the province, especially in east and southeast regions (Fig. 5l, m). This is likely due to the bias associated with higher resolution processes represented by RCMs compared to GCMs and the amplified error of RCMs from the driving GCM.

3.1.4 Green water

The SWAT simulation results show a wide range of green water flow (GWF) between 107 mm in the western part and 500 mm in the agricultural lands in the southern part of the province (Fig. 6a) for the historical period. Projected future changes in GWF indicated a likely increase of between 1 and 100 mm for GCMs-RCP 2.6-D-S1, GCMs-RCP 2.6-D-S2, and GCMs-RCP 8.5-D-S1 scenarios. The projected increases (Fig. 6b–d) in most of the central sub-basins are consistent

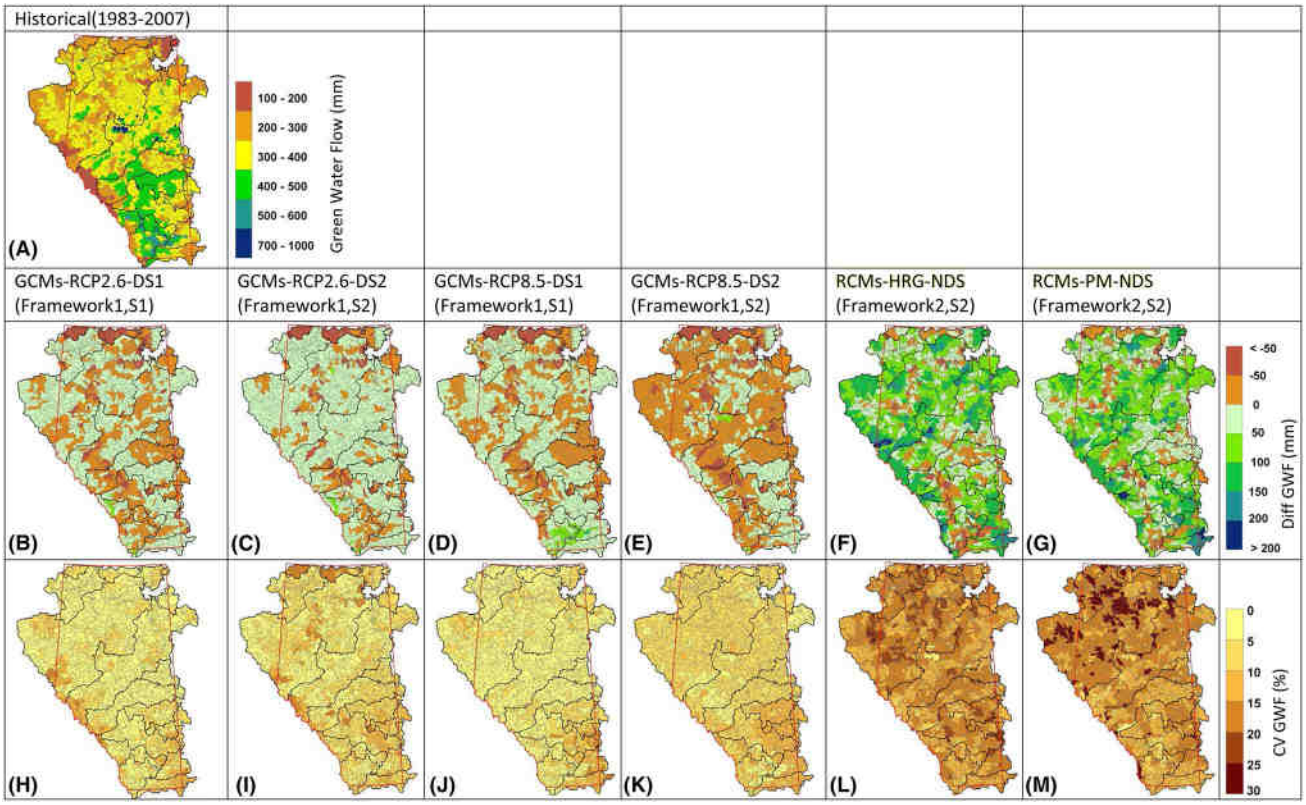

Fig. 6 Spatial distribution of annual green water flow for historical period (1983–2007) (**a**), its changes (Changes = [[future values − historical values]/historical values] × 100) between the near future (2010–2035) and historical period (**b, d**), and between far future (2040–2065) and historical period (**c, e**) calculated using ensemble of GCMs-bias corrected data under RCP 2.6 and RCP 8.5 scenarios, respectively. **f, g** The spatial distribution of changes between 2040 and 2065 and historical period calculated using an ensemble of RCMs using Hargreaves and Penman–Monteith evapotranspiration calculation methods respectively. The coefficient of variation, indicating inter-model variation, for the near future (**h, j**), far future (**i, k**) under the RCP 2.6 and RCP 8.5 scenarios, respectively. **l, m** The coefficient of variation for RCM models projections using Hargreaves and Penman–Monteith evapotranspiration calculation methods respectively

with the projected decreases in blue water (Fig. 5b–d). Green water flow increases due to warmer conditions, especially in agricultural regions. This limits the available water that can contribute to blue water. The ensemble results of GCMs-RCP 8.5-D-S2 show a probable decrease for most sub-basins in the province, except those located in the southeast part of Alberta (Fig. 6e). Projected rising temperature with an average of 3 °C in GCMs-RCP 8.5-D-S2 scenarios is the main reason for increased GWF for most parts of the province. In RCM-Har-D-S2 and RCM-Pen-D-S2 scenarios, likely increases of up to 150 mm and 210 mm are projected for the southeast and mountainous regions of the province, respectively (Fig. 6f, g). The magnitude of spatial variation of GWF differed significantly from GCMs (with SD of 28–30 mm) to RCMs (with SD of 86–116 mm). The results of GCM CV showed that disagreement among the GCMs is seen in the west, south, and southeast of the province (Fig. 6h–j). Similar to other hydrologic components from RCMs, both RCM-Har-D-S2 and RCM-Pen-D-S2 scenarios showed higher variation (2–3 times more) between RCM models (Fig. 6l, m).

Figure 7 shows the spatial distribution of the annual available green water storage (GWS) for the historical period and the changes in the future (S1 and S2). Historically, the annual GWS varies from 0 mm in the southeast part of the province up to more than 600 mm in the northwest of Alberta. However, there are some sub-basins in the province with historical GWS beyond 600 mm (Fig. 7a). Areas with larger GWS and smaller coefficient of variation have a higher potential for development of rainfed (green) agriculture. Our GWS projections for the near future showed likely increases in most of the southern sub-basins, and potential decreases in some northern sub-basins for RCP2.6-D-S1, RCP2.6-D-S2, and RCP8.5-D-S1 (Fig. 7b–d). In RCP8.5-D-S2, results showed an average increase of 23 mm (Table SI.3) for most of the sub-basins in the province (Fig. 7e). These overall increases in GWS are consistent with the increases in precipitation and blue water (Figs. 3e, 5e) and the decrease

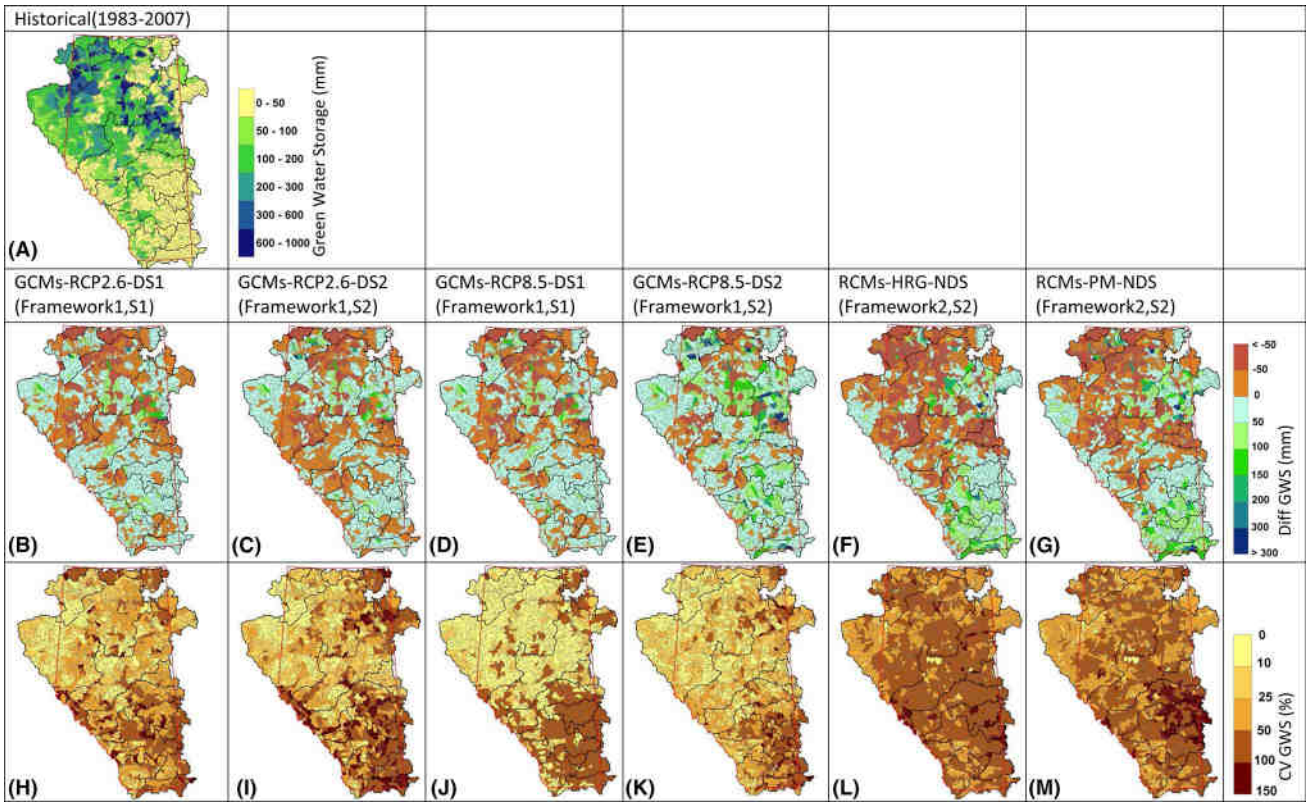

Fig. 7 Spatial distribution of annual green water storage for historical period (1983–2007) (**a**), its changes (Changes = [[future values − historical values]/historical values]×100) between near future (2010–2035) and historical period (**b, d**), and between far future (2040–2065) and historical period (**c, e**) calculated using ensemble of GCMs-bias corrected data under RCP 2.6 and RCP 8.5 scenarios, respectively. **f, g** The spatial distribution of changes between 2040 and 2065 and historical period calculated using an ensemble of RCMs using Hargreaves and Penman–Monteith evapotranspiration calculation methods respectively. The coefficient of variation, indicating inter-model variation, for the near future (**h, j**), far future (**i, k**) under the RCP 2.6 and RCP 8.5 scenarios, respectively. **l, m** The coefficient of variation for RCM models projections using Hargreaves and Penman–Monteith evapotranspiration calculation methods respectively

in green water flow (Fig. 6e). In both RCM-Har-D-S2 and RCM-Pen-D-S2 scenarios, results indicated a likely increase of 100–160 mm for the southern sub-basins and a probable decrease of 5–60 mm for most of the northern and western sub-basins. Although the spatial distribution of projected changes in GWS were close in both RCM-Har-D-S2 and RCM-Pen-D-S2, the former predicted slightly more decrease in GWS compared to the latter (Fig. 6f, g). Figure 7h–m present the analysis of CVs related to GWS. Similar to other hydro-climatic variables, the CV between GCMs (Fig. 7h–k) were smaller than CV between RCMs (Fig. 7l, m). This finding is in line with our other results. Overall, smaller CV was found in the GCMs-RCPs scenarios in the northern part of the province and larger CV was obtained in southern areas.

3.2 Seasonal analysis of blue and green water

We aggregated the simulated monthly blue and green water components from sub-basin scale to the provincial level to assess the seasonal differences between three scenario-sets. For the sake of brevity, the results for framework-1, scenario-set1 are provided in Supplemental Information (Figures SI.3 and SI.4). Figure 8a, b present future projections of monthly blue water compared to the baseline at three quantile levels for framework-1, scenario-set2 and framework-2, scenario-set3 as defined in Table 5. Since the results are based on the median of ensemble of models, they do not reflect the uncertainty of individual climate models. In these graphs uncertainty range is calculated based on the differences between the quantities depicted by various lines (solid, dash, and dash-dot) and colors (black, red, blue, green) explained in the figure legends.

In general, the results (Fig. 8a) showed large differences between 2.5, 50 and 97.5 quantiles of blue water due to model parameter uncertainty. The comparison of blue water calculated from historical simulations of GCMs (yellow lines) and those simulated using the observed historical climate data (black lines) showed a similar pattern at the $Q_{2.5}$, Q_{50}, and $Q_{97.5}$ levels with slight underestimation in historical GCMs simulations from April to September.

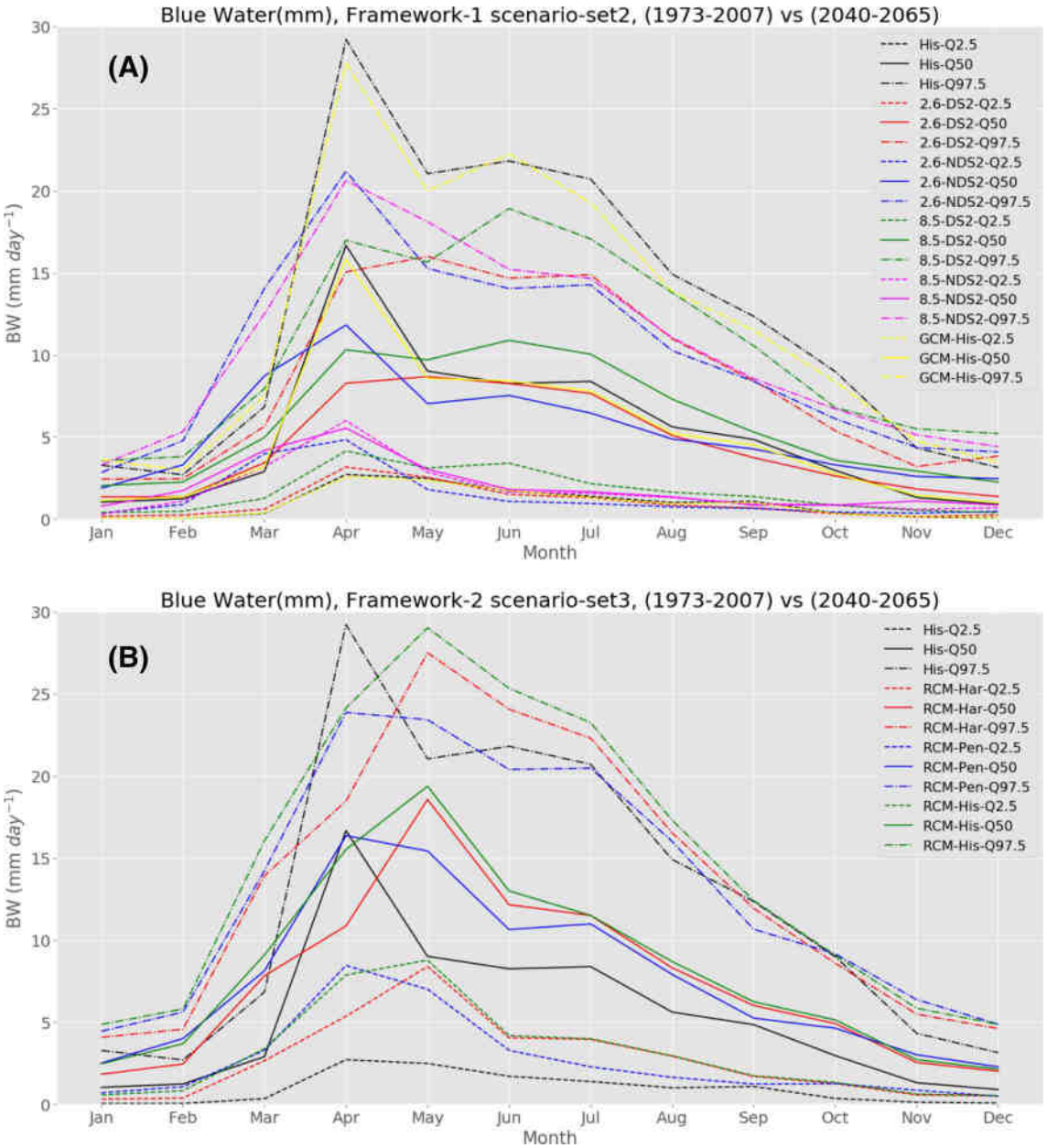

Fig. 8 Long-term monthly blue water under framework 1 (**a**), scenario-set2; and framework 2, scenario-set3 (**b**) as defined in Table 5. Solid lines represent the blue water values at 50th percentile, dashed lines represent the blue water values at 2.5th percentile, dashed-dotted lines represent the green water flow values at 97.5th percentile. Black lines represent historical observed scenarios. In **a** red lines represent RCP2.6 downscaled scenarios, blue line represent original RCP2.6 simulations without further bias correction at local scale, Green lines represent RCP8.5 downscaled scenarios, pink lines represent original RCP8.5 simulations without further bias correction at local scale, and Yellow lines represent the historical simulation of GCMs. In **b** black lines represent historical observed scenarios, red lines represent RCMs simulations using Hargreaves evapotranspiration calculation method, blue lines represent RCMs simulations using Penman–Monteith evapotranspiration calculation method, and green lines represent RCMs historical simulations (ensemble of seven sets of RCMs and using Hargreaves method)

The projected results of blue water for the framework-1, scenario-set2, i.e. GCMs-RCP(2.6/8.5)-(D/ND)-S2, showed increases in February and March, and decreases from April to September at the $Q_{97.5}$ and Q_{50} levels as compared to the historical values (except RCP 8.5-ND-S2 at the level of 50th percentile). The blue water results at $Q_{2.5}$ level showed increases from October to April, while they remained stable from May to September. In framework-1, scenario-set2, most fluctuations are seen in April, where for instance the uncertainty range due to HM-P and HM-R

varies between 2.5 and 28 mm in historical scenarios (differences between dot-black and dash-dot-black lines). For the framework-2 scenario-set3 (Fig. 8b), the future simulated blue water using the RCMs was projected to increase as compared to that of using observed climate data in all months except April at the Q_{50}level. However, it was projected to be stable at the $Q_{97.5}$ level in all months, except April and May where fluctuations are significant. Comparison of the simulated blue water using RCM data for both future and historical periods (only plotted for ensemble of seven available RCMs out of ten green lines), showed a decreasing pattern for blue water resources. Nevertheless, the large uncertainty inherent in RCMs projections for western Canada, especially for precipitation (Mearns et al. 2012), necessitates removal of the RCM error before using them in regional climate-impact studies.

We investigated seasonal variability of green water flow across Alberta for the historical period and future scenarios and demonstrated our results in Fig. 9a, b and Figure SI.4. The long-term monthly averages of green water flow in framework-1 scenario-set2 showed that the uncertainty due to HM-P and HM-R is dominant from April to September as compared to the uncertainty due to the selection of different RCPs and BCDS. For instance, in July the uncertainty associated with HM-P and HM-R for future scenario ranges from 23.5 to 29.5 mm for framework-1 scenario-set2, while uncertainty range due to the selection of RCPs and BSDS is 1–3 mm and 2–4 mm, respectively (Fig. 9a). The share of RCPs and BCDS sources on the overall uncertainty band of green water flow is dominant in June and August (Fig. 9a). The comparison of green water simulated based on historical GCMs data with that of simulated using observed records showed an overall agreement in Fig. 9a and Figure SI. 4. In the framework-2 scenario-set3, the uncertainty range of green water flow due to HM-P and HM-R sources is 0.5–28 mm for $Q_{97.5}$, (with the minimum range in January and the maximum range in July) while this range for selection of ET methods is 2–7 mm, with the maximum value projected for the month of June for $Q_{97.5}$ values (Fig. 9b). From November to March, the uncertainty caused by model parameter is similar to the uncertainty caused by selection of RCPs and BCDS methods. This is supported by small distances between future projections (Fig. 9b). Results showed an increase in future green water as compared to the simulation using observed data. To justify the magnitude of increase in green water, we plotted the green water results of historical simulations of RCMs (only plotted for ensemble of seven available RCMs out of ten green lines) and compared with the green water results of observed simulation. The results showed a general overestimation of green water in historical RCMs compared to the observed simulation (Fig. 9b).

3.3 Evaluation of the sources of uncertainty

We analyzed the seasonal uncertainty decomposition of blue and green water components (Figs. 10, 11). Figure 10a–c indicate that the hydrological model parameters (including both HM-P and HM-R) are the dominant source of uncertainty for blue water from April to September in all frameworks and scenario-sets (see Tables 6, 7 for more details). Our uncertainty decomposition results revealed that the contributions of HM-P and HM-R to the overall uncertainty were from 11% in February to 41% in April in framework-1 scenario-set1, i.e. GCMs-RCPs (2.6/8.5)-(D/ND)-S1 (Fig. 10a). The results showed that in framework-1 scenario-set2, i.e. GCMs-RCPs (2.6/8.5)-(D/ND)-S2, the share of HM-P and HM-R uncertainty were from 15% (February) to 33% (April) in overall uncertainty. In the framework-2, scenario-set3, i.e. RCMs-D-S2, the HM-P, and HM-R contributed between 35% (December) to 48% (April) to the overall uncertainty. The contribution of the hydro-climatic nonlinearity behavior, demonstrated by the interaction term, i.e. Equation 8 and Eq. 15; to the overall uncertainty of blue water varied between 6–14 and 7–14% throughout the year for scenario-set1 and scenario-set2, respectively (Fig. 10a, b). For the combination of RCMs-ET methods (framework-2 scenario-set3), the interaction term was up to 4% for all months. It is noteworthy that we performed two independent ANOVA-SUFI-2 analysis using (1) absolute values of future simulations (ten sets of RCMs; Fig. 10c), and (2) differences of future and historical simulations (seven sets of RCMs; Figure SI.5A) of blue water in the RCMs framework. Only seven historical simulations of RCMs were available at the time running the scenarios. The results of uncertainty decomposition using the absolute values revealed that RCMs contribute 51.1% to the total uncertainty on the average (see Table 6 Farmework-2 Scenarios-set3). However, this value represents a combined error due to model bias in simulation of historical climate, and that of climate change signal. In the second approach, we applied the ANOVA-SUFI-2 on the changes of future and historical simulations of ensemble of seven RCMs. The results showed a decrease in contribution of the RCMs to 36.67% (see Table 6 Farmework-2 Scenarios-set3, numbers reported in brackets), which is more reasonable and consistent with the GCMs results (Table 6 Farmewirk-1 Scenarios-set1 and Farmework-1 Scenarios-set2).

Figure 11a–c showed that the climate models (i.e. GCMs and RCMs), and the HM-P and HM-R were the main contributors to the overall uncertainty of green water flow projections. We found that from April (32% in framework1-scenario set1 and 36% in framework1-scenario set2) to August (38% in framework1-scenario set1 and 35% in framework1-scenario set2), the HM-P and HM-R were dominant sources of uncertainty in scenario-set1 and scenario-set2 (Fig. 11a,

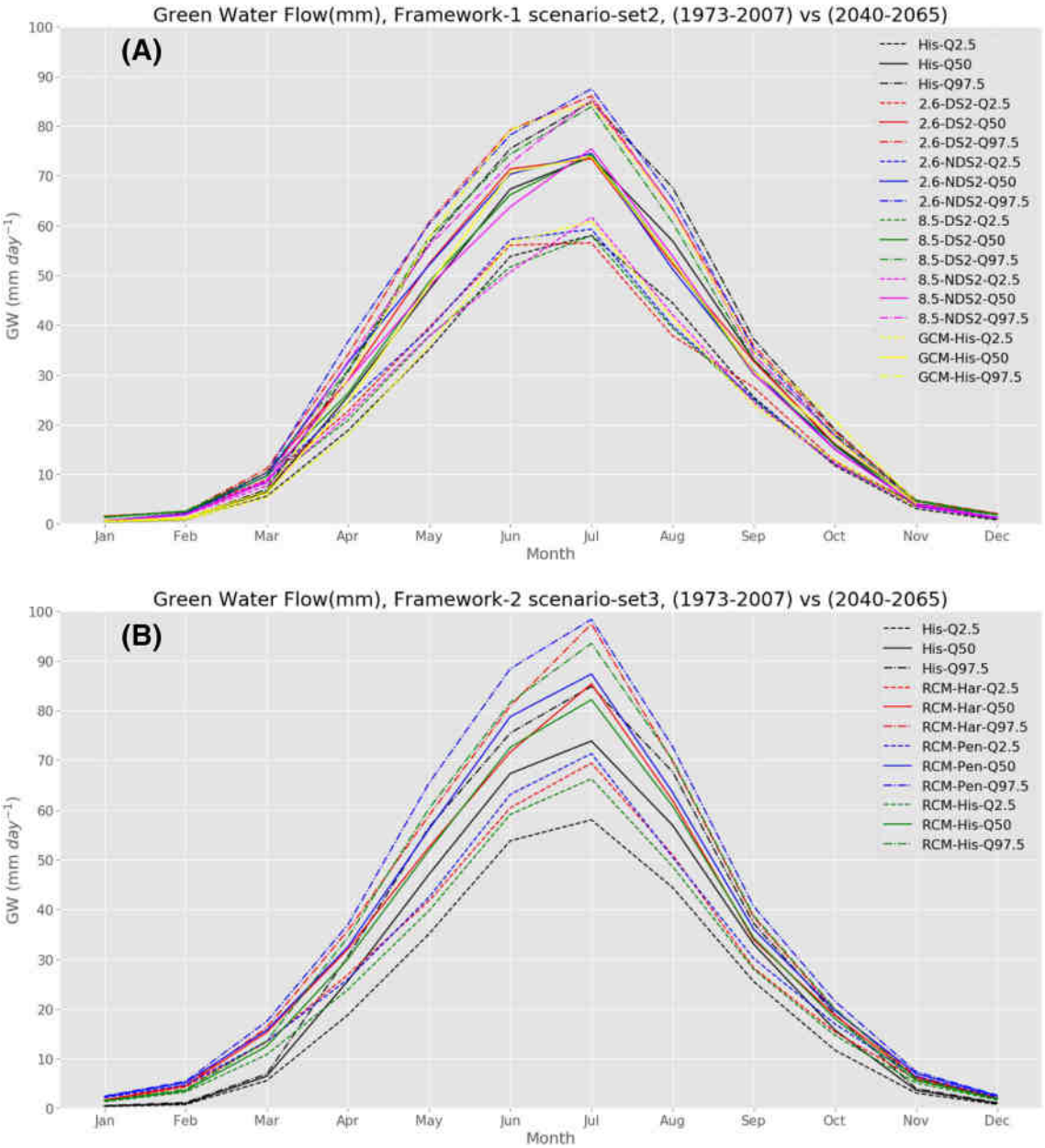

Fig. 9 Long-term monthly green water flow (i.e. actual evapotranspiration) under framework 1, scenario-set2 (**a**); and framework 2, scenario-set3 (**b**) as defined in Table 5. Solid lines represent the green water flow values at 50th percentile, dashed lines represent the green water flow values at 2.5th percentile, and dashed-dotted lines represent the green water flow values at 97.5th percentile. Black lines represent historical observed scenarios. In **a** red lines represent RCP2.6 downscaled scenarios, blue line represent original RCP2.6 simulations without further bias correction at local scale, green lines represent RCP8.5 downscaled scenarios, pink lines represent original RCP8.5 simulations without further bias correction at local scale, and yellow lines represent the historical simulation of GCMs. In **b** black lines represent historical observed scenarios, red lines represent RCMs simulations using Hargreaves evapotranspiration calculation method, blue lines represent RCMs simulations using Penman–Monteith evapotranspiration calculation method, and green lines represent RCMs historical simulations (ensemble of seven sets of RCMs and using Hargreaves method)

b), followed by uncertainty associated with GCMs in these scenarios (18–30% in scenario-set1 and 25–31% in scenario-set2). In scenario-set1 and scenario-set2, the contribution of both GCMs and hydrological model parameters in the overall uncertainty were similar from October to March. From October to March, the contribution of HM-P and HM-R decreased in scenario-set1 (Fig. 11a), while the share of RCPs and BCDS increased for the same scenarios (Fig. 11b). In the framework-2, scenario-set3, RCMs had the most influence (40%), followed by the HM-P and HM-R

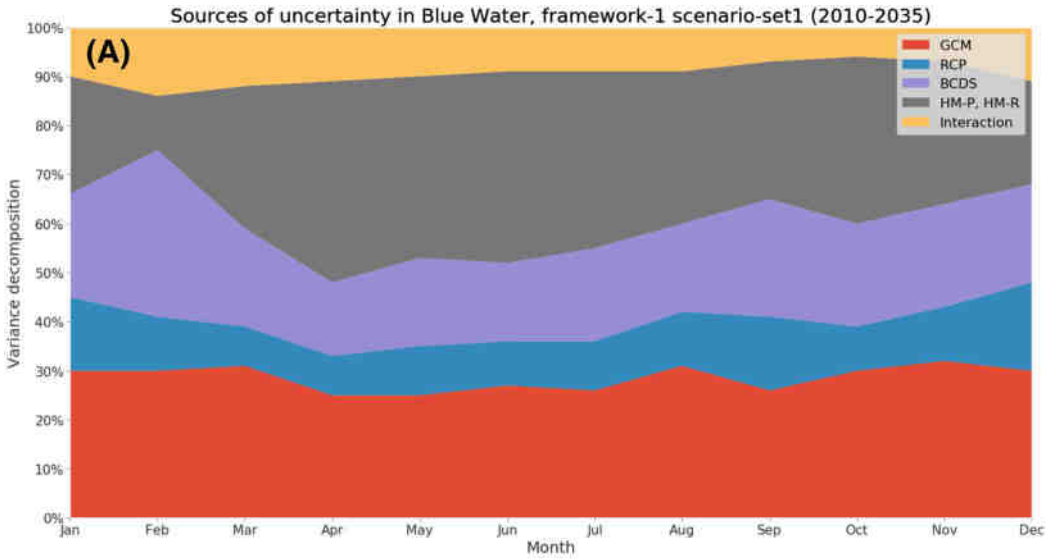
Sources of uncertainty in Blue Water, framework-1 scenario-set1 (2010-2035)
(A)
GCM
RCP
BCDS
HM-P, HM-R
Interaction
Variance decomposition
100%
90%
80%
70%
60%
50%
40%
30%
20%
10%
0%
Jan
Feb
Mar
Apr
May
Jun
Jul
Aug
Sep
Oct
Nov
Dec
Month

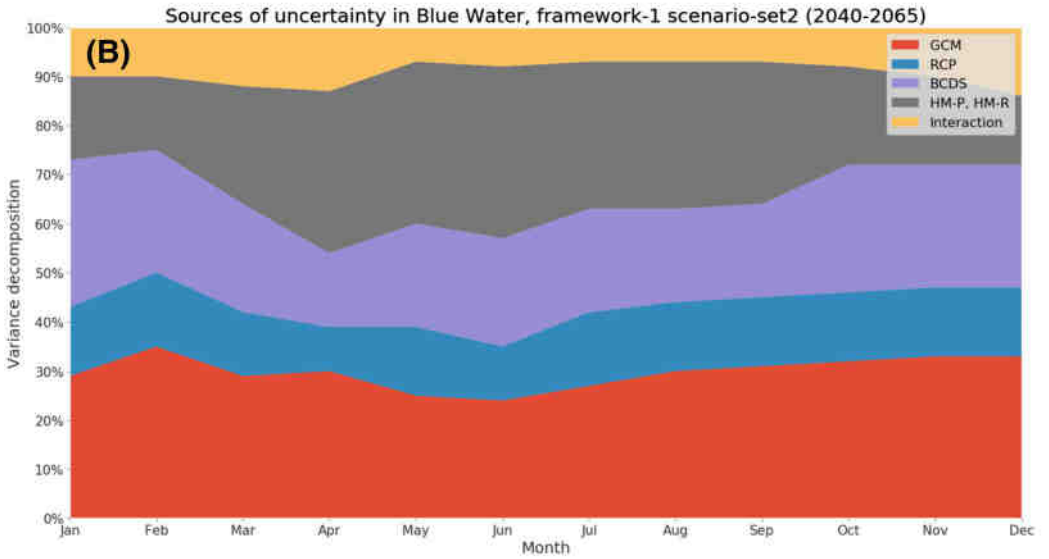
Sources of uncertainty in Blue Water, framework-1 scenario-set2 (2040-2065)
(B)
GCM
RCP
BCDS
HM-P, HM-R
Interaction
Variance decomposition
100%
90%
80%
70%
60%
50%
40%
30%
20%
10%
0%
Jan
Feb
Mar
Apr
May
Jun
Jul
Aug
Sep
Oct
Nov
Dec
Month

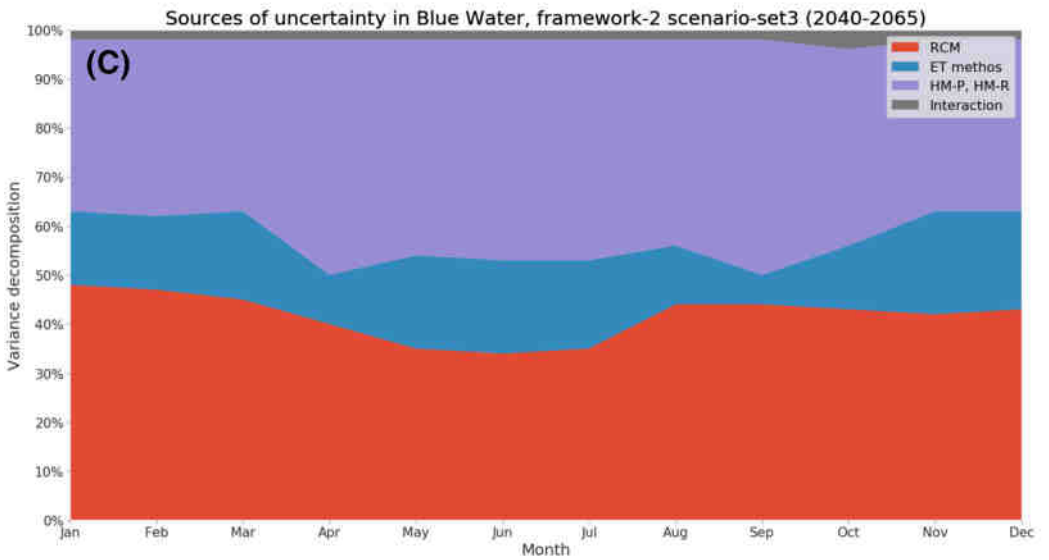
Sources of uncertainty in Blue Water, framework-2 scenario-set3 (2040-2065)
(C)
RCM
ET methos
HM-P, HM-R
Interaction
Variance decomposition
100%
90%
80%
70%
60%
50%
40%
30%
20%
10%
0%
Jan
Feb
Mar
Apr
May
Jun
Jul
Aug
Sep
Oct
Nov
Dec
Month

◂**Fig. 10** Variance decomposition of the uncertainty in blue water for Alberta under three sets of scenarios: Framework-1 scenario-set1 (**a**), framework-1 scenario-set2 (**b**), and framework-2 scenario-set3 (**c**). The uncertainty sources are GCMS, RCPs, BCDS, HM-P and HM-R, RCMs, and ET calculation methods. The differences of future and historical simulations of blue water (ensemble of nine sets of GCMs) were used for the uncertainty decomposition of GCMs framework (**a, b**). The absolute values of future simulations of blue water (ensemble of ten sets of RCMs) used for the uncertainty decomposition of RCMs framework (**c**)

(26%), and the ET calculation methods (22.3%) as the uncertainty sources (Table 6; Fig. 11c).

The interaction term contribution to the overall uncertainty of green water flow varied between 6–13% and 8–14% throughout the year for scenario-set1 and scenario-set2, respectively (Fig. 11a, b). For scenario-set3 of the RCMs-ET methods, the interaction term contributed 5–16% to the overall uncertainty (Fig. 11c). Similar to blue water, we preformed two independent ANOVA-SUFI-2 analyses on green water flow in the framework-2-scenario-set3 using (1) absolute values for ten RCMs (Fig. 11c), and (2) differences of historical and future simulations, i.e. delta values, for seven RCMs (Figure SI.5 B). Comparison of the results indicated that share of uncertainty contributed from RCMs decreased by using delta instead of absolute values. This was similar to our findings in decomposition analysis of blue water availability, and resulted in an increase in contribution of other sources in the overall uncertainty cascade (see Table 6 Farmewirk-2 Scenarios-set3).

We summarized the results of uncertainty decomposition in Tables 6 and 7. In general, the dominant sources of uncertainty in framework-1 scenario-set1 and scenario-set2 were hydrological model parameters followed by GCMs. In framework-2 scenario-set3, the main sources of uncertainty were associated with RCMs followed by hydrological model parameters. Uncertainty assessment of blue water showed that the share of HM-R and HM-P varies between 13%-40% in the overall cascade of uncertainty while for green water flow HM-R and HM-P contribute between 11%-41% in different months (Table 7). Our results showed that RCPs and BCDS have similar quantity of contribution in the overall cascade of uncertainty, and the interaction source has the minimum share compared to other sources in framework-1 scenario-set1 and framework-1 scenario-set2.. In framework-2 scenario-set3, RCMs source was the dominant share, followed by HM-R and HM-P, ET methods and interaction sources.

3.4 Caveats

The approach and the frameworks developed in this study provide novel basis to examine contribution of the hydrological model parameterization and regionalization in the full cascade of uncertainty. However, similar to other studies, our work might have some limitations. For instance, we did not consider various methods of bias correction and downscaling (i.e., BCCA, quantile regression, etc.) in the design of our two frameworks. In addition, we only chose SWAT model, as one of the widely used hydrologic models to study the effects of HM-P and HM-R in the overall cascades of uncertainty. Further research is needed to assess the share of other hydrologic models such as VIC, HBV, WasSIM-ETH, etc. in the entire cascade of uncertainty. Moreover, in the RCMs framework, we used the absolute values of future simulations of ten RCM for the ANOVA analysis. Although this approach has incidences in literature (Vetter et al. 2017), it may lead to error in uncertainty decomposition of framework-2, since it reflects a mixed share of model bias (i.e. simulation during historical period), and error in projection of climate change response. To address this we applied the ANOVA-SUFI-2 on the differences of future and historical simulations of RCMs (similar to the GCMs framework) only for seven sets out of ten RCMs, where data were available at the time of scenario analysis. In doing so, the magnitude of model error in RCMs framework was eliminated from the uncertainty decomposition results.

4 Summary and conclusions

The goal of this study was to quantify the contribution of hydrological model parameterization and regionalization along with other drivers in the overall cascade of uncertainty in climate change impact projections. We developed a new coupled ANOVA-SUFI-2 approach for decomposition analysis of ancertainty associated with the impact of climate change on hydro-climatic variables. We used a previously calibrated SWAT model of Alberta, which has been parameterized and regionalized over 2255 subbasins in Alberta. We analyzed different hydro-climatic variables including precipitation, mean temperature, blue water, green water flow, and green water storage using an ensemble of nine GCMs, two RCPs, two BCDS methods, ten sets of RCMs, and two evapotranspiration calculation methods resulting in a total of 92 individual climate-impact SWAT models. We compared our projected results between future scenarios (2010–2035 and 2040–2065) and the historical period 1983–2007. We evaluated the projected changes of hydro-climatic variables at three quintile levels, i.e. 2.5%, 50%, and 97.5%. We categorized our 92 models in three scenario-sets under two frameworks to determine the share of different uncertainty sources in the overall uncertainty in the projection of blue and green water resources. The ANOVA-SUFI-2 coupled approach, allowed quantification of uncertainty resulting from hydrologic model parameterization and

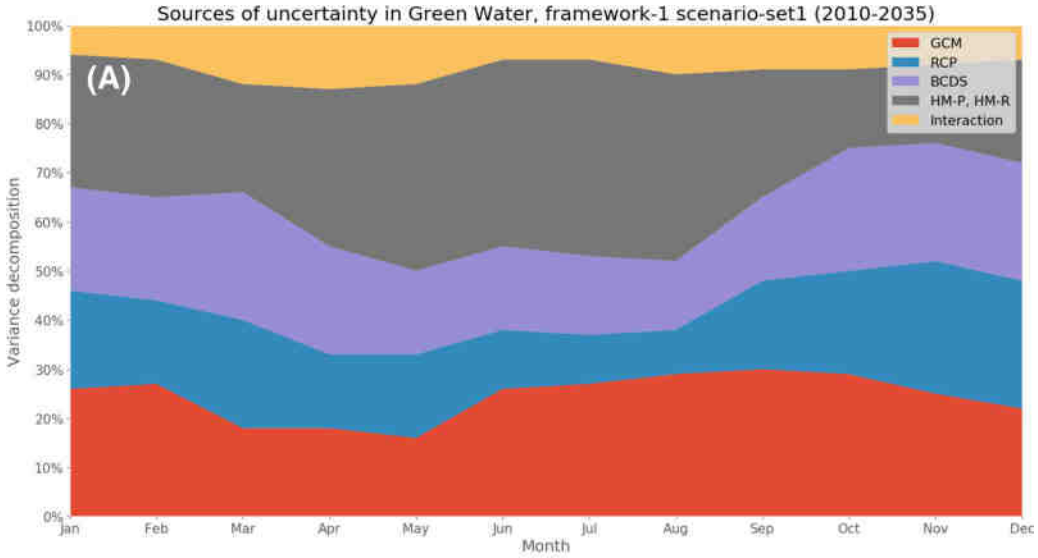
Sources of uncertainty in Green Water, framework-1 scenario-set1 (2010-2035)
(A)
GCM
RCP
BCDS
HM-P, HM-R
Interaction
Variance decomposition
Month
Jan
Feb
Mar
Apr
May
Jun
Jul
Aug
Sep
Oct
Nov
Dec

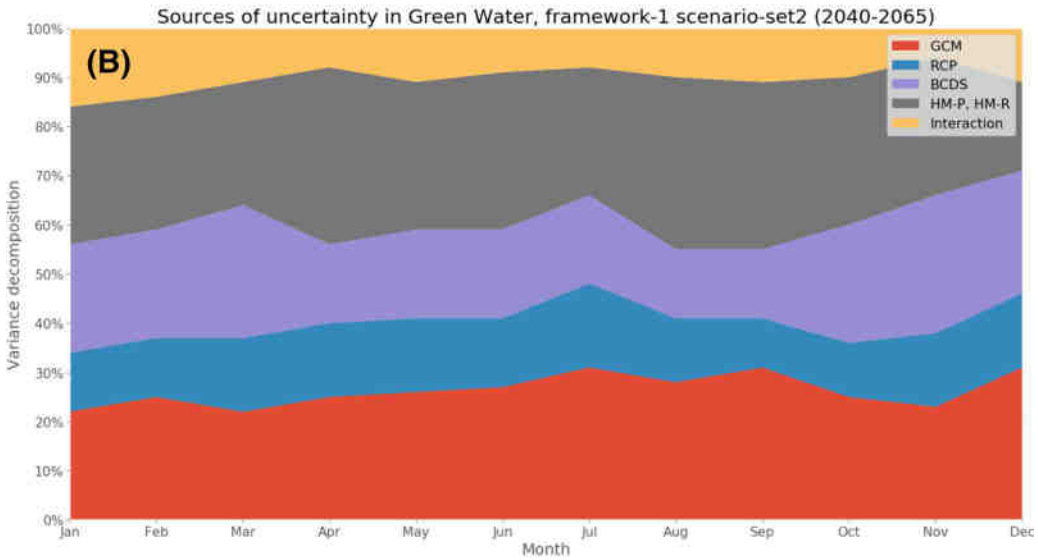
Sources of uncertainty in Green Water, framework-1 scenario-set2 (2040-2065)
(B)
GCM
RCP
BCDS
HM-P, HM-R
Interaction
Variance decomposition
Month

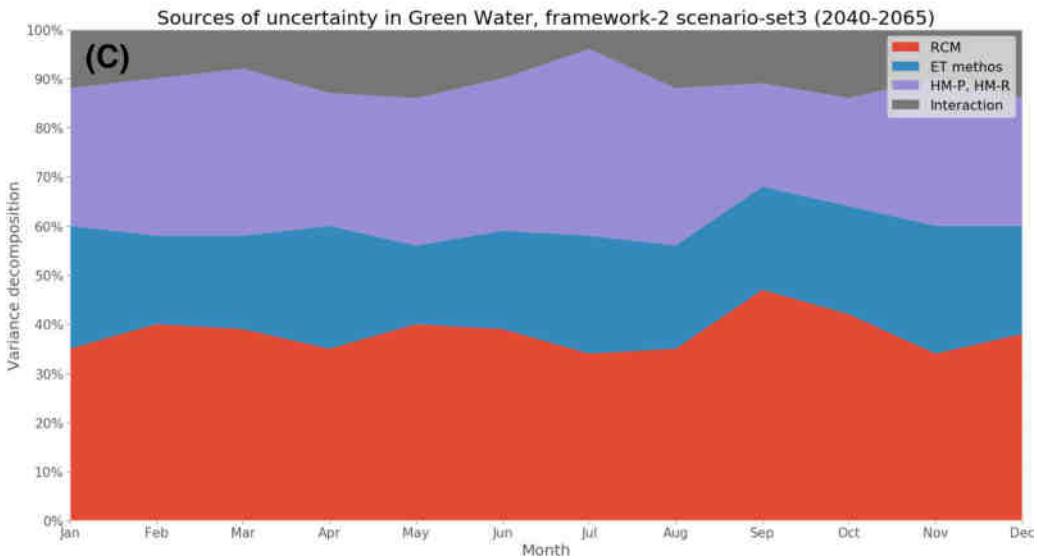
Sources of uncertainty in Green Water, framework-2 scenario-set3 (2040-2065)
(C)
RCM
ET methos
HM-P, HM-R
Interaction
Variance decomposition
Month

◂**Fig. 11** Variance decomposition of the uncertainty in green water flow for Alberta under seven sets of scenarios: framework-1 scenario-set1 (**a**), framework-1 scenario-set2 (**b**), and framework-2 scenario-set3 (**c**). The uncertainty sources are GCMS, RCPs, BCDS, HM-P and HM-R, RCMs, and ET calculation methods. The differences of future and historical simulations of green water flow (ensemble of nine sets of GCMs) were used for the uncertainty decomposition of GCMs framework (**a, b**). The absolute values of future simulations of green water flow (ensemble of ten sets of RCMs) were used for the uncertainty decomposition of RCMs framework (**c**)

Table 6 The contribution of different sources of uncertainty to the overall cascade

Scenario-set	Blue water (%)	Green water flow (%)
Framework-1, scenario-set1		
GCMs	28.58	24.42
RCPs	11.25	17.83
BCDS methods	20.58	20.32
HM-P and HM-R	30.02	28.52
Interaction	9.67	8.91
Framework-1, scenario-set2		
GCMs	29.83	26.34
RCPs	13.41	13.67
BCDS methods	22.5	20.53
HM-P and HM-R	24.83	29.08
Interaction	9.58	10.58
Framework-2, scenario-set3		
RCMs	51.1 (36.67)	40.0 (33.16)
ET methods	7.1 (17.16)	22.3 (23.24)
HM-P and HM-R	38.3 (42.33)	26.0 (30.9)
Interaction	3.5 (3.84)	11.8 (12.7)

For the framework-2, scenario-set3, numbers in the brackets are contributions from seven RCMs using delta values

regionalization, along with other sources including climate models, greenhouse gas emission scenarios, bias correction and downscaling methods, evapotranspiration calculation methods, and their interactions.

We acknowledge other similar studies that quantified different sources of uncertainty in the impact assessments (Hattermann et al. 2017). However, in the vast majority of earlier studies, the share of uncertainty caused by HM-P and HM-R is not quantified in future impact assessments. The novelty of our ANOVA-SUFI-2 approach is its capability to analyze HM-P and HM-R while assessing other sources in the uncertainty cascade.

Using ANOVA-SUFI-2 method we found that the climate models and hydrological model parameterization and regionalization are the dominant sources of the uncertainty. The share of uncertainty varied over different seasons. We found that during spring and summer seasons the climate models are the second largest contributors to the overall uncertainty. For the winter and spring, the contribution of HM-P and HM-R decreased, while other sources shared more uncertainty in overall cascade. In general, our results showed a higher discrepancy between RCMs results (from NARCCAP) compared to GCMs results (from PCIC). This is likely because of the inconsistency in the biases due to representation of physical processes in RCM and GCMs, which were also addressed by other researchers (Erler and Peltier 2017; Fernández et al. 2018). Our results showed that there is a slightly higher agreement among climate model projections in near future scenarios compared to the far future, which is in line with the finding of other researchers (Krysanova and Hattermann 2017; Vetter et al. 2017).

Considering the substantial impacts of natural variability on the uncertainty of climate-impact projections, which is an intrinsic property of the natural climate system, efforts should be made to better represent the characteristics of the natural and decal variability. To better understand this phenomena we refer readers to some important contribution to the literature such as Hawkins and Sutton (2011), Deser et al. (2012) and Erler et al. (2015). One of the key drivers of uncertainty in southern Alberta is likely the Pacific Decadal Oscillation (PDO, Lapp et al. 2013). To account for the effects of PDO, integration of algorithms into existing models is necessary and it helps better characterization of natural/decadal variability. Improving the representation of the PDO would require a better representation of the relevant physics and dynamics in climate models.

Overall, a large share of HM-P and HM-R in the cascade of uncertainty in climate-impact projections, may raise an argument that using a highly parametrized physical model such as SWAT could be subjective in climate change impact studies. The application of such models could be limited if the initial SWAT model of a watershed was not set up consciously and uncertainty range of parameters was wide. This has been addressed in the literature (Abbaspour et al. 2017; Faramarzi et al. 2015), which leads to the challenge of decision making under uncertainty condition. We recommend to use similar framework as the one developed in this study to investigate other similar spatial-data demanding and physical-based models such as VIC, Noah-MP, CLM, or HydroGeoSphere in climate-impact projections and to investigate the sensitivity of different hydrological models (HM-S) in the analysis of the uncertainty cascade. It might be possible that more physic-based models such as Noah-MP would probably show less parameter uncertainty in comparison with SWAT. However, a robust assessment using a similar approach as this study is required for robust conclusion.

Table 7 Minimum, maximum, and overal contribution of hydrologic model parameters, i.e. HM-P and HM-R, in overall uncertainty cascade

Scenarios	Green water flow			Blue water		
	Min (%)	Max (%)	Range (%)	Min (%)	Max (%)	Range (%)
Framework-1, scenario-set1	16	44	28	11	41	30
Framework-1, scenario-set2	11	47	36	14	35	21
Framework-2, scenario-set3	21	38	17	35	48	13

Our approach is not unique to Alberta and should be applied in other jurisdictions around the world. Defining different sources of uncertainty will help decision makers and scientists to better deal with the issue of uncertainty and also help to identify the necessary research and/or data acquisition required to reduce uncertainty and improve decision confidence.

Acknowledgements We gratefully acknowledge the funding from Alberta Innovates (Grant # RES0030781) and the grant awarded by the Campus Alberta Innovation Program Chair (Grant #RES0030781). The authors would like to acknowledge the anonymous reviewer who made a detailed evaluation on the paper.

References

Abbaspour KC, Yang J, Maximov I, Siber R, Bogner K, Mieleitner J, Zobrist J, Srinivasan R (2007) Modelling hydrology and water quality in the pre-ailpine/alpine Thur watershed using SWAT. J Hydrol 333:413–430

Abbaspour KC, Faramarzi M, Ghasemi SS, Yang H (2009) Assessing the impact of climate change on water resources in Iran. Water Resour Res. https://doi.org/10.1029/2008WR007615

Abbaspour KC, Rouholahnejad E, Vaghefi S, Srinivasan R, Yang H, Klove B (2015) A continental-scale hydrology and water quality model for Europe: calibration and uncertainty of a high-resolution large-scale SWAT model. J Hydrol 524:733–752

Abbaspour K, Vaghefi S, Srinivasan R (2017) A guideline for successful calibration and uncertainty analysis for soil and water assessment: a review of papers from the 2016 international SWAT conference. Water 10:6

Arnell NW (1999) Climate change and global water resources. Global environmental change. Pergamon, Bergama, pp S31–S49

Arnell NW, Gosling SN (2016) The impacts of climate change on river flood risk at the global scale. Clim Change 134:387–401

Arnold JG, Srinivasan R, Muttiah RS, Williams JR (1998) Large area hydrologic modeling and assessment—Part 1: model development. J Am Water Resour Assoc 34:73–89

Arnold JG, Moriasi DN, Gassman PW, Abbaspour KC, White MJ, Srinivasan R, Santhi C, Harmel RD, van Griensven A, Van Liew MW, Kannan N, Jha MK (2012) SWAT: model use, calibration, and validation. Trans ASABE 55:1491–1508

Asong ZE, Khaliq MN, Wheater HS (2016) Multisite multivariate modeling of daily precipitation and temperature in the Canadian Prairie Provinces using generalized linear models. Clim Dyn 47:2901–2921

Barnett TP, Adam JC, Lettenmaier DP (2005) Potential impacts of a warming climate on water availability in snow-dominated regions. Nature 438:303–309

Bavay M, Grunewald T, Lehning M (2013) Response of snow cover and runoff to climate change in high Alpine catchments of Eastern Switzerland. Adv Water Resour 55:4–16

Beniston M (2012) Impacts of climatic change on water and associated economic activities in the Swiss Alps. J Hydrol 412:291–296

Beven K, Binley A (1992) The future of distributed models: model calibration and uncertainty prediction. Hydrol Process 6:279–298

Bosshard T, Carambia M, Goergen K, Kotlarski S, Krahe P, Zappa M, Schär C (2013) Quantifying uncertainty sources in an ensemble of hydrological climate-impact projections. Water Resour Res 49:1523–1536

Cannon AJ (2015) Selecting GCM scenarios that span the range of changes in a multimodel ensemble: application to cmip5 climate extremes indices. J Clim 28:1260–1267

Chen J, Brissette FP, Leconte R (2011a) Uncertainty of downscaling method in quantifying the impact of climate change on hydrology. J Hydrol 401:190–202

Chen J, Brissette FP, Poulin A, Leconte R (2011b) Overall uncertainty study of the hydrological impacts of climate change for a Canadian watershed. Water Resour Res 47:16

Chen J, Brissette FP, Chaumont D, Braun M (2013) Performance and uncertainty evaluation of empirical downscaling methods in quantifying the climate change impacts on hydrology over two North American river basins. J Hydrol 479:200–214

Deque M, Rowell DP, Luthi D, Giorgi F, Christensen JH, Rockel B, Jacob D, Kjellstrom E, de Castro M, van den Hurk B (2007) An intercomparison of regional climate simulations for Europe: assessing uncertainties in model projections. Clim Change 81:53–70

Deser C, Phillips A, Bourdette V, Teng HY (2012) Uncertainty in climate change projections: the role of internal variability. Clim Dyn 38:527–546

Duan QY, Gupta VK, Sorooshian S (1993) Shuffled complex evolution approach for effective and efficient global minimization. J Optim Theory Appl 76:501–521

Erler AR, Peltier WR (2016) Projected changes in precipitation extremes for western Canada based on high-resolution regional climate simulations. J Clim 29:8841–8863

Erler AR, Peltier WR (2017) Projected hydroclimatic changes in two major river basins at the Canadian west coast based on high-resolution regional climate simulations. J Clim 30:8081–8105

Erler AR, Peltier WR, D'Orgeville M (2015) Dynamically downscaled high-resolution hydroclimate projections for western Canada. J Clim 28:423–450

Falkenmark M, Rockström J (2006) The new blue and green water paradigm: breaking new ground for water resources planning and management. J Water Resour Plan Manag 132:129–132

Fan FX, Bradley RS, Rawlins MA (2015) Climate change in the Northeast United States: an analysis of the NARCCAP multimodel simulations. J Geophys Res Atmos 120:10569–10592

Faramarzi M, Abbaspour KC, Schulin R, Yang H (2009) Modelling blue and green water resources availability in Iran. Hydrol Process 23:486–501

Faramarzi M, Srinivasan R, Iravani M, Bladon KD, Abbaspour KC, Zehnder AJB, Goss GG (2015) Setting up a hydrological model of

Alberta: data discrimination analyses prior to calibration. Environ Modell Softw 74:48–65

Faramarzi M, Abbaspour KC, Adamowicz WL, Lu W, Fennell J, Zehnder AJB, Goss GG (2017) Uncertainty based assessment of dynamic freshwater scarcity in semi-arid watersheds of Alberta, Canada. J Hydrol Reg Stud 9:48–68

Fernández J, Frías MD, Cabos WD, Cofiño AS, Domínguez M, Fita L, Gaertner MA, García-Díez M, Gutiérrez JM, Jiménez-Guerrero P, Liguori G, Montávez JP, Romera R, Sánchez E (2018) Consistency of climate change projections from multiple global and regional model intercomparison projects. Clim Dyn. https://doi.org/10.1007/s00382-018-4181-8

Fortin V (2000) Le modèle météo-apport HSAMI: historique, théorie et application. Rapport de recherche, revision 1.5. Institut de recherche d'Hydro-Québec, Varennes, p 68

Fortin JP, Turcotte R, Massicotte S, Moussa R, Fitzback J, Villeneuve JP (2001) Distributed watershed model compatible with remote sensing and GIS data. I: description of model. J Hydrol Eng 6:91–99

Freni G, Mannina G, Viviani G (2009) Urban runoff modelling uncertainty: comparison among Bayesian and pseudo-Bayesian methods. Environ Modell Softw 24:1100–1111

Gao P, Carbone GJ, Guo DS (2016) Assessment of NARCCAP model in simulating rainfall extremes using a spatially constrained regionalization method. Int J Climatol 36:2368–2378

Gobiet A, Kotlarski S, Beniston M, Heinrich G, Rajczak J, Stoffel M (2014) 21st century climate change in the European Alps—a review. Sci Total Environ 493:1138–1151

Gualdi S, Somot S, May W, Castellari S, Déqué M, Adani M, Artale V, Bellucci A, Breitgand JS, Carillo A, Cornes R, Dell'Aquila A, Dubois C, Efthymiadis D, Elizalde A, Gimeno L, Goodess CM, Harzallah A, Krichak SO, Kuglitsch FG, Leckebusch GC, L'Hévéder B, Li L, Lionello P, Luterbacher J, Mariotti A, Navarra A, Nieto R, Nissen KM, Oddo P, Ruti P, Sanna A, Sannino G, Scoccimarro E, Sevault F, Struglia MV, Toreti A, Ulbrich U, Xoplaki E (2013) Future climate projections. In: Navarra A, Tubiana L (eds) Regional assessment of climate change in the mediterranean: volume 1: air, sea and precipitation and water. Springer Netherlands, Dordrecht, pp 53–118

Hallegatte S (2009) Strategies to adapt to an uncertain climate change. Glob Environ Change Hum Policy Dimens 19:240–247

Harding BL, Wood AW, Prairie JR (2012) The implications of climate change scenario selection for future streamflow projection in the Upper Colorado River Basin. Hydrol Earth Syst Sci 16:3989–4007

Hargreaves GL, Hargreaves George H, Riley JP (1985) Agricultural benefits for senegal river basin. J Irrig Drain Eng 111:113–124

Hattermann FF, Krysanova V, Gosling SN, Dankers R, Daggupati P, Donnelly C, Flörke M, Huang S, Motovilov Y, Buda S, Yang T, Müller C, Leng G, Tang Q, Portmann FT, Hagemann S, Gerten D, Wada Y, Masaki Y, Alemayehu T, Satoh Y, Samaniego L (2017) Cross-scale intercomparison of climate change impacts simulated by regional and global hydrological models in eleven large river basins. Clim Change 141:561–576

Hattermann FF, Vetter T, Breuer L, Buda S, Daggupati P, Donnelly C, Fekete B, Flörke F, Gosling SN, Hoffmann P, Liersch S, Masaki Y, Motovilov Y, Müller C, Samaniego L, Stacke T, Wada Y, Yang T, Krysnaova V (2018) Sources of uncertainty in hydrological climate impact assessment: a cross-scale study. Environ Res Lett 13:015006

Hawkins E, Sutton R (2011) The potential to narrow uncertainty in projections of regional precipitation change. Clim Dyn 37:407–418

Haydon S, Deletic A (2009) Model output uncertainty of a coupled pathogen indicator—hydrologic catchment model due to input data uncertainty. Environ Modell Softw 24:322–328

Hewitt AJ, Booth BBB, Jones CD, Robertson ES, Wiltshire AJ, Sansom PG, Stephenson DB, Yip S (2016) Sources of uncertainty in future projections of the carbon cycle. J Clim 29:7203–7213

IPCC (2013) Climate change 2013: the physical science basis. In: Stocker TF, Qin D, Plattner G-K, Tignor M, Allen SK, Boschung J, Nauels A, Xia Y, Bex V, Midgley PM (eds) Contribution of working group I to the fifth assessment report of the intergovernmental panel on climate change. Cambridge University Press, Cambridge, p 1535

Jeong DI, Sushama L, Naveed Khaliq M (2014) The role of temperature in drought projections over North America. Clim Change 127:289–303

Jiang P, Yu ZB, Gautam MR, Yuan FF, Acharya K (2016) Changes of storm properties in the United States: observations and multimodel ensemble projections. Global Planet Change 142:41–52

Jiang RG, Gan TY, Xie JC, Wang N, Kuo CC (2017) Historical and potential changes of precipitation and temperature of Alberta subjected to climate change impact: 1900–2100. Theor Appl Climatol 127:725–739

Kay AL, Davies HN, Bell VA, Jones RG (2009) Comparison of uncertainty sources for climate change impacts: flood frequency in England. Clim Change 92:41–63

Krysanova V, Hattermann FF (2017) Intercomparison of climate change impacts in 12 large river basins: overview of methods and summary of results. Clim Change 141:363–379

Kuczera G, Kavetski D, Franks S, Thyer M (2006) Towards a Bayesian total error analysis of conceptual rainfall-runoff models: characterising model error using storm-dependent parameters. J Hydrol 331:161–177

Laflamme EM, Linder E, Pan Y (2016) Statistical downscaling of regional climate model output to achieve projections of precipitation extremes. Weather Clim Extrem 12:15–23

Lapp SL, St. Jacques J-M, Sauchyn DJ, Vanstone JR (2013) Forcing of hydroclimatic variability in the northwestern Great Plains since AD 1406. Quat Int 310:47–61

Maheu A, St-Hilaire A, Caissie D, El-Jabi N, Bourque G, Boisclair D (2016) A regional analysis of the impact of dams on water temperature in medium-size rivers in eastern Canada. Can J Fish Aquat Sci 73:1885–1897

Masud MB, McAllister T, Cordeiro MRC, Faramarzi M (2018) Modeling future water footprint of barley production in Alberta, Canada: implications for water use and yields to 2064. Sci Total Environ 616–617:208–222

McKay MD, Beckman RJ, Conover WJ (1979) A comparison of three methods for selecting values of input variables in the analysis of output from a computer code. Technometrics 21:239–245

McKay MD, Beckman RJ, Conover WJ (2000) A comparison of three methods for selecting values of input variables in the analysis of output from a computer code. Technometrics 42:55–61

Mearns LO, Gutowski W, Jones R, Leung R, McGinnis S, Nunes A, Qian Y (2009) A regional climate change assessment program for north America. Eos Trans Am Geophys Union 90:311

Mearns LO, Arritt R, Biner S, Bukovsky MS, McGinnis S, Sain S, Caya D Jr, Flory JC, Gutowski D, Takle W, Jones ES, Leung R, Moufouma-Okia R, McDaniel W, Nunes L, Qian AMB, Roads Y, Sloan J, Snyder L M (2012) The North American regional climate change assessment program: overview of phase I results. Bull Am Meteorol Soc 93:1337–1362

Mearns LO, Sain S, Leung LR, Bukovsky MS, McGinnis S, Biner S, Caya D, Arritt RW, Gutowski W, Takle E, Snyder M, Jones RG, Nunes AMB, Tucker S, Herzmann D, McDaniel L, Sloan L (2013) Climate change projections of the North American Regional Climate Change Assessment Program (NARCCAP). Clim Change 120:965–975

Mearns LO et al (2014) The North American regional climate change assessment program dataset. National Center for Atmospheric Research Earth System Grid data portal, Boulder

Montanari A (2007) What do we mean by 'uncertainty'? The need for a consistent wording about uncertainty assessment in hydrology. Hydrol Process 21:841–845

Morgan MG, Henrion M (1990) Uncertainty: a guide to dealing with uncertainty in quantitative risk and policy analysis. Cambridge University Press, Cambridge

Moss RH, Edmonds JA, Hibbard KA, Manning MR, Rose SK, van Vuuren DP, Carter TR, Emori S, Kainuma M, Kram T, Meehl GA, Mitchell JFB, Nakicenovic N, Riahi K, Smith SJ, Stouffer RJ, Thomson AM, Weyant JP, Wilbanks TJ (2010) The next generation of scenarios for climate change research and assessment. Nature 463:747–756

Nakicenovic N, Alcamo J, Grubler A, Riahi K, Roehrl R, Rogner H-H, Victor N (2000) Special report on emissions scenarios (SRES), a special report of Working Group III of the intergovernmental panel on climate change. Cambridge University Press, Cambridge

O'Neill BC, Kriegler E, Riahi K, Ebi KL, Hallegatte S, Carter TR, Mathur R, van Vuuren DP (2014) A new scenario framework for climate change research: the concept of shared socioeconomic pathways. Clim Change 122:387–400

O'Neill BC, Kriegler E, Ebi KL, Kemp-Benedict E, Riahi K, Rothman DS, van Ruijven BJ, van Vuuren DP, Birkmann J, Kok K, Levy M, Solecki W (2017) The roads ahead: narratives for shared socioeconomic pathways describing world futures in the 21st century. Glob Environ Change 42:169–180

Pacific Climate Impacts Consortium, University of Victoria (2014) Statistically downscaled climate scenarios. https://www.pacificclimate.org/data/statistically-downscaled-climate-scenarios. Accessed 1 Mar 2017

Penman HL (1948) Evaporation in nature. Rep Progr Phys XI:366–388

Poulin A, Brissette F, Leconte R, Arsenault R, Malo J-S (2011) Uncertainty of hydrological modelling in climate change impact studies in a Canadian, snow-dominated river basin. J Hydrol 409:626–636

Prudhomme C, Davies H (2009) Assessing uncertainties in climate change impact analyses on the river flow regimes in the UK. Part 2: future climate. Clim Change 93:197–222

Räty O, Räisänen J, Ylhäisi JS (2014) Evaluation of delta change and bias correction methods for future daily precipitation: intermodel cross-validation using ENSEMBLES simulations. Clim Dyn 42:2287–2303

Riahi K, Rao S, Krey V, Cho CH, Chirkov V, Fischer G, Kindermann G, Nakicenovic N, Rafaj P (2011) RCP 8.5-A scenario of comparatively high greenhouse gas emissions. Clim Change 109:33–57

Roop S, Guiling W, Miao Y, Jeehee K (2015) Comparison of RCM and GCM projections of boreal summer precipitation over Africa. J Geophys Res Atmos 120:3679–3699

Salazar E, Hammerling D, Wang X, Sanso B, Finley AO, Mearns LO (2016) Observation-based blended projections from ensembles of regional climate models. Clim Change 138:55–69

Schar C, Ban N, Fischer EM, Rajczak J, Schmidli J, Frei C, Giorgi F, Karl TR, Kendon EJ, Tank A, O'Gorman PA, Sillmann J, Zhang XB, Zwiers FW (2016) Percentile indices for assessing changes in heavy precipitation events. Clim Change 137:201–216

Seneviratne SI, Donat MG, Pitman AJ, Knutti R, Wilby RL (2016) Allowable CO_2 emissions based on regional and impact-related climate targets. Nature 529:477–483

Teklesadik AD, Alemayehu T, van Griensven A, Kumar R, Liersch S, Eisner S, Tecklenburg J, Ewunte S, Wang X (2017) Inter-model comparison of hydrological impacts of climate change on the Upper Blue Nile basin using ensemble of hydrological models and global climate models. Clim Change 141:1–16

Thiemann M, Trosset M, Gupta H, Sorooshian S (2001) Bayesian recursive parameter estimation for hydrologic models. Water Resour Res 37:2521–2535

Vaghefi SA, Abbaspour N, Kamali B, Abbaspour KC (2017) A toolkit for climate change analysis and pattern recognition for extreme weather conditions—case study: California-Baja California Peninsula. Environ Modell Softw 96:181–198

van Vuuren DP, Stehfest E, den Elzen MGJ, Kram T, van Vliet J, Deetman S, Isaac M, Goldewijk KK, Hof A, Beltran AM, Oostenrijk R, van Ruijven B (2011) RCP2.6: exploring the possibility to keep global mean temperature increase below 2 degrees C. Clim Change 109:95–116

van den Bergh JCJM (2017) A third option for climate policy within potential limits to growth. Nature Clim Change 7:107–112

Vetter T, Huang S, Aich V, Yang T, Wang X, Krysanova V, Hattermann F (2015) Multi-model climate impact assessment and intercomparison for three large-scale river basins on three continents. Earth Syst Dyn 6:17–43

Vetter T, Reinhardt J, Flörke M, van Griensven A, Hattermann F, Huang S, Koch H, Pechlivanidis IG, Plötner S, Seidou O, Su B, Vervoort RW, Krysanova V (2017) Evaluation of sources of uncertainty in projected hydrological changes under climate change in 12 large-scale river basins. Clim Change 141:419–433

von Storch H, Zwiers FW (1999) Statistical analysis in climate research. Cambridge Univ. Press, Cambridge

Wagener T, McIntyre N, Lees MJ, Wheater HS, Gupta HV (2003) Towards reduced uncertainty in conceptual rainfall-runoff modelling: dynamic identifiability analysis. Hydrol Process 17:455–476

Wilby RL, Harris I (2006) A framework for assessing uncertainties in climate change impacts: low-flow scenarios for the River Thames, UK. Water Resour Res. https://doi.org/10.1029/2005WR004065

Yip S, Ferro CAT, Stephenson DB, Hawkins E (2011) A simple, coherent framework for partitioning uncertainty in climate predictions. J Clim 24:4634–4643